Time-space variations in the East African Rift magmatism: the role of different mantle domains

Time-space variations in the East African Rift magmatism: the role of different mantle domains

Journal:	*Italian Journal of Geosciences*
Manuscript ID	IJG-2022-1046.R1
Manuscript Type:	Original Article
Date Submitted by the Author:	n/a
Complete List of Authors:	Bragagni, Alessandro Braschi, Eleonra; Consiglio Nazionale delle Ricerche, Istituto di Geoscienze e Georisorse, Sezione di Firenze Orlando, Andrea Corti, Giacomo; CNR, Tommasini, Simone; Università degli Studi di Firenze, Dipartimento di Scienze della Terra
Keywords:	East African Rift System, rift-related volcanism, Upper mantle domains, Radiogenic isotopes

Time-space variations in the East African Rift magmatism: the role of different mantle domains

Alessandro Bragagni[1,*], Eleonora Braschi[2,*], Andrea Orlando[2], Luisa Guarnieri[1], Giacomo Corti[2], Simone Tommasini[1,#]

1 Dipartimento di Scienze della Terra, Università degli Studi di Firenze, Via Giorgio La Pira, 4, 50121, Firenze, Italy
2 Consiglio Nazionale delle Ricerche – Istituto di Geoscienze e Georisorse, Sede Secondaria di Firenze, Via Giorgio La Pira, 4, 50121, Firenze, Italy

** these authors contributed equally*
 # corresponding author

Abstract

The East African Rift System (EARS) is the classic example of an active continental rift where extensional tectonics and lithospheric thinning have been closely associated to the generation of large volumes of magmas and represents the environment with the largest range of erupted magma types all over the world. The geochemical signature of erupted magmas testifies the involvement of different mantle domains and depths (i.e., subcontinental lithosphere, asthenosphere and deeper mantle sources). Our aim is to investigate the variable contribution of different mantle domains in the genesis of the EARS magmas through space and time, considering not only the geochemical signature of erupted magmas but also the geochemical message of mantle xenoliths. The main goal is to provide a large-scale view of the common process driving the origin of magmas in the EARS beyond the local peculiarities linked to specific settings. To this aim, we screened an exhaustive geochemical database of basalts and mantle xenoliths from the EARS, and we report original trace element and Sr-Nd isotope data of new samples collected from the Main Ethiopian Rift and Turkana depression. The data were subdivided according to spatial and temporal criteria. From a spatial point of view, the samples were ascribed to five groups, namely: Afar, Ethiopia, Turkana, Eastern Branch, and Western Branch; from a temporal point of view, the magmatic activity of the EARS was subdivided into three main temporal intervals: 45-25 Ma, 25-10 Ma and 10-0 Ma. The geochemical and radiogenic isotope (Sr, Nd, Pb) signature of the selected basalts denotes the variable contributions of a mantle plume, a more depleted asthenospheric mantle (DMM), and different SubContinental Lithospheric Mantle (SCLM) domains, depending on their temporal and spatial distribution. The geochemistry of the selected basalts shows a marked correspondence with the compositional heterogeneity of mantle xenoliths, whose isotopic systematics (Sm-Nd, Re-Os) indicates the formation of the local SCLM in the Archean and during the Pan-African orogeny. Both SCLM domains contributed significantly to

magma genesis in the Western Branch (whose signature points towards a contribution of the Pan-African lithosphere) and Eastern Branch (which is also affected by Archean SCLM domains) magmas. The contribution of the SCLM generally increases with time, possibly related to an increase of the geothermal gradient in response to the arrival and flattening of the plume head at the base of the lithosphere and later extension, thinning and shallower melting. Our interpretation supports a pivotal role of the different SCLM domains in magma genesis that is able to fully explain the large compositional heterogeneity of the EARS basalts and represents a reasonable alternative to the putative presence of multiple mantle plumes or a heterogeneous mantle upwelling.

Keywords: East African Rift System; rift-related volcanism; upper mantle domains; radiogenic isotopes

1. Introduction

Deformation and thinning of the lithosphere and magma generation with related volcanic activity are typical expressions of extensional forces on continental plates (e.g., Ebinger, 2020). Extension-related deformation results in the formation of systems of normal faults and subsiding basins; magma generation, migration and uprising may lead to the development of volcanic systems and/or magmatic underplating. Both these major processes may significantly vary in different rift systems or even within a single rift, and during progressive rift evolution.

The East African Rift System (EARS; Fig. 1) is an ideal place to investigate extensional deformation, thinning of the continental lithosphere, and magma generation, along with their mutual interactions and variations in space and time (e.g., Furman, 2007; Rooney, 2017, 2020a,b,c,d; Biggs et al., 2021; Morley and Chantraprasert, 2022). The rift is indeed characterised by significant time and spatial variations in deformation style, lithosphere extension and magma volumes and composition (e.g., Ebinger, 2020).

Many previous studies have highlighted the occurrence of different sources in the magmatism of the EARS, including deep mantle plume material, depleted asthenospheric mantle (DMM-like) and the SubContinental Lithospheric Mantle (SCLM). The exact nature of these sources and their variable contribution in the magma genesis is debated and hard to define, and it is beyond the aim of this paper to provide a comprehensive review of the complex magmatic processes that accompanied the development of the EARS, for which the reader is addressed to the recent, comprehensive works by Rooney (2017, 2020a,b,c,d). Instead, the goal of this work is to analyse the available trace element and isotopic data on volcanic rocks from the EARS to derive a scenario of the time-space variations

of major mantle processes associated with rifting such as lithospheric modification and melting. Although rift lavas may display a significant variability at a local scale (see for instance the diversity of volcanic products of the Western Branch in terms of major element composition and isotopic signature; e.g., Furman et al., 2006) we grouped the available data in different large-scale sectors of the EARS, and long-time intervals, to isolate the common mantle processes controlling rift-related volcanism in relation to the different tectonic settings and stages of rift development. In addition, our approach was integrated with an analysis of available mantle xenoliths from the whole African domains; the occurrence of mantle xenoliths in many volcanoes of the rift system provides indeed the opportunity to study the geochemical and isotopic characteristics of the different SCLM domains and their potential contribution to the EARS magmatism.

Based on this large-scale approach, we discuss a geodynamic scenario which accounts for the spatio-temporal variations of the role of some important processes (e.g., plume and plate dynamics) on the generation of magmas in the EARS.

2. Geodynamic setting

Extension in East Africa and surrounding regions is controlled by interaction among three major plates: Africa, Arabia and Somalia (e.g., Chorowitz, 2005). The long-lasting motion of the Africa and Somalia, with intervening minor plates south of the Turkana depression, controls extensional deformation in the EARS, whereas extension in the Gulf of Aden, Red Sea and the Afar depression is controlled by the motion of Arabia with respect to the Africa-Somalia system.

At its northern termination, the EARS is connected to the oceanic domains of the Gulf of Aden and Red Sea by the Afar depression, which hosts the triple junction between the African, Arabian and Somalian plates. In Afar, the crust has been significantly thinned (up to possibly less than ~15 km), the lithosphere is hot and thin and a focused tectono-magmatic activity within axial magmatic segments has been suggested to document incipient oceanic spreading (e.g., Bastow and Keir, 2011). South of Afar, the EARS is expressed by the occurrence of the Main Ethiopian Rift (MER), where significant axial tectono-magmatic activity in the northern sector testifies ongoing magma intrusion and significant magmatic modification of the lithosphere (e.g., Keranen et al., 2004). Important magmatic underplating results in a still rather thick crust in the MER (thickness up to >30km).

The MER terminates in the south, in the Turkana depression, a lowland where faulting and volcanic activity are widespread over an area up to >300 km wide. The anomalous breath of the deformed region and the characteristics of the tectonic activity in the area have been generally related to a thin crust (20-25 km) resulting from a Mesozoic-Early Cenozoic extension event which gave rise to NW-SE trending basins (e.g., Anza and South Sudan grabens; Corti et al., 2022 and references therein).

South of the Turkana depression, the rift bifurcates because of the thick and strong Tanzanian craton, forming the Eastern and Western Branches. The Eastern Branch is composed of the Kenya Rift and Tanzania Divergence, whereas the Western Branch is made of major rift basins such as Albertine, Tanganyika and Malawi. Both rift arms are localised within old mobile belts (such as the Mozambique belt). Similarly to the MER, the Eastern Branch is characterised by significant volcano-tectonic activity, which is localised within axial segments in the northern part of the Kenya rift (e.g., Muirhead et al., 2022). Rifting in this EARS branch has likely propagated southwards, with its youngest expression located on the south-eastern side of the thick Tanzania craton, where the deformation zone widens to form the Tanzania Divergence (e.g., Ebinger et al., 1997).

The Western Branch is made of a series of long, deep basins formed in Proterozoic-Paleozoic orogenic belts at the western side of the Tanzanian craton. Geophysical data and models indicate that the lithosphere in this region is still cold and strong and values of bulk extension in these basins are smaller than other sectors of the EARS. However, recent works (Hopper et al., 2020) imaged a significant lithospheric thinning and modification, in the absence of elevated temperatures and magmatism. Indeed, unlike other sectors of the EARS, most of the basins in the Western rift lack any expression of volcanic activity; the four major volcanic provinces (Kivu, Rungwe, Toro-Ankole, Virunga) seem to be localised within regional transfer zones connecting major basins.

Overall, geophysical studies reveal significant variations in characteristics of the lithosphere in these different domains of the EARS, with thickness varying from >100 km in Proterozoic and Archean lithospheres (up to ~180-250 km in old cratonic cores), to generally less than 100 km within the rifts (e.g., Fishwick, 2010; Fishwick and Bastow, 2011). Lithospheric thickness is generally higher beneath the Western Branch than in other areas (e.g., Fishwick and Bastow, 2011; Nijnju et al., 2019), although thinning to 50-60 km has been imaged in the northern Malawi rift (Hopper et al., 2020). Lateral variations in lithospheric strength (i.e., between the old cratons and the surrounding Pan-African mobile belts) strongly controlled the localization of extensional deformation in large parts of the EARS.

2.1. Deformation and basin evolution in the EARS

Cenozoic extensional deformation in East Africa is characterised by a complex spatial-temporal evolution (see for instance Purcell, 2017 for a comprehensive review). Following the Mesozoic-Early Cenozoic phase of graben development, deformation continued in the Turkana depression during the Eocene-Oligocene; the other portions of the future EARS lack evidence of significant faulting and rift-related subsidence at that time. Deformation started during Late Oligocene along the western and southern Afar margins, as a consequence of a westward rift propagation from the eastern parts of the

Gulf of Aden caused by counterclockwise rotation of the Arabian plate (Zwaan et al., 2020). Similarly, normal faulting and subsidence continued in the Turkana depression, but significant deformation still lacked in both Eastern and Western Branches. Tectonic activity increased in the Early Miocene (post-22 Ma): deformation in Ethiopia gave rise the initial development of the southern Main Ethiopian Rift (MER), whereas south of the Turkana depression rifting propagated to form portions of the northern Kenya Rift (Purcell, 2017); some deformation could have affected limited portions of the Western Branch (Simon et al., 2017). A major phase of rifting commenced at around 10-15 Ma, with development of different basins in the Western Branch (e.g., Albertine, Kivu, Tanganyika), subsidence and faulting in the northern MER and southward propagation of the Kenya Rift. Significant deformation continued in the Late Miocene-Pliocene up to recent times. Important subsidence affected the narrow rift valleys of the Western Branch; the Eastern Branch further propagated southwards, with the rift impinging the thick lithosphere of the Tanzanian Craton (Masai block) and creating a region of distributed deformation in the so-called Tanzanian Divergence; rifting accelerated in the wide deformation zone of the Turkana depression where the Kenyan and Ethiopian rifts progressively linked; rifting and tectono-magmatic activity increased markedly in the Kenya Rift, in Afar and in the MER, where large boundary faults accommodated deformation, later replaced by axial systems of faulting and volcanism.

Overall, there are significant spatial variations in the timing of extension initiation, with the likely heterogeneous, limited activation of individual basins up to after 10-15 Ma, when more diffuse and continuous extension affected the whole EARS in response to motion between the major Nubia-Somalia plates. Rifting has progressed to focused axial tectono-magmatic activity in parts of the rift (northern Ethiopia and northern Kenya), indicating an advanced rifting stage, and almost break-up and incipient spreading in Afar, where the lithosphere is thin and hot. In other parts of the EARS (e.g., Western Branch) rifting is in its initial stages, and occurs in still thick and cold lithosphere.

2.2. Volcanic activity

The initial phases of Cenozoic volcanism in East Africa correspond to the eruption of flood basalts in the Horn of Africa (see review in Rooney, 2017). This large-scale volcanism started in southern Ethiopia and northern Kenya at ~45 Ma until ~34 Ma, followed by a second pulse of flood basalts during the Oligocene, with eruption of thick lava flows characterising the plateaus of northern Ethiopia, Somalia and Yemen (Rooney, 2017 and references therein). This phase of flood basalt activity occurred between ~34 Ma and ~27 Ma, with the majority of volcanic products emplaced in a short time span at ~30 Ma (Hoffman et al, 1997). Another, significantly less important phase of basaltic volcanism occurred between ~27 Ma and ~22 Ma throughout the northern EARS (Early

Miocene Resurgence Phase of Rooney, 2020a), and this activity produced shield-volcanoes until about 10 Ma in the plateaus of Ethiopia (Kieffer et al., 2004). Limited eruption of carbonatitic magmas in the Western rift occurred in this period (~25-26 Ma) close to Lake Rukwa area (Roberts et al., 2012). The resurgence phase in the EARS may have continued in an additional phase of widespread basaltic activity which took place between 20 and 16 Ma in the Northern Kenya Rift, southern Ethiopia, and parts of the Turkana depression (Rooney, 2020a). This phase, dominated by basaltic volcanism was followed by a period of widespread evolved volcanism consisting of phonolites in northern Kenya, and explosive silicic eruptions in the Main Ethiopian Rift. Alkaline volcanism initiated in the Western Branch, specifically in the Kivu-Virunga and Rukwa volcanic provinces.

At ~12 Ma a renewed phase of widespread basaltic volcanism (Mid-Miocene Resurgence Phase of Rooney, 2020a) characterised East Africa from Afar to Kenya, with activity in the south slightly predating equivalent basaltic volcanism in the north. This phase of dominantly basaltic activity lasted until ~8-9 Ma and was followed by widespread bimodal volcanism (basalts, trachytes and large-scale silicic volcanism) concomitant with a major rifting episode characterising the subsiding rift valleys of Ethiopia and Kenya, and by focused volcanic activity in the different volcanic provinces of the Western Branch.

Another major pulse of basaltic activity commenced at about ~4 – 5 Ma in the Afar depression, with the eruption of the so-called Afar Stratoid Series, which affected most of the depression until the Pleistocene. Widespread late Miocene-Pliocene basaltic lavas also interested the Turkana depression (Franceschini et al., 2020; Rooney, 2020a). Recent volcanic activity is mostly bimodal in the Ethiopian and Kenyan rifts, with axial silicic central volcanoes, in most cases with caldera-forming eruptions, and alignments of basaltic cones and fissures. Basaltic activity is predominant in the northern Afar depression, where incipient continental break-up is observed at axial tectono-magmatic segments. Magma intrusion in the lithosphere and the related thermo-mechanical effects may have favoured magma-assisted rifting in these regions (e.g., Kendall et al., 2005) and weakened the lithosphere to allow rifting in strong cratonic lithosphere of the southern parts of the EARS (such as the Tanzanian Divergence; e.g., Ebinger, 2020).

Overall, the strong difference in the volumes of magmatic products between the highly volcanic Eastern Branch and the almost non-volcanic Western Branch has been interpreted to reflect an asymmetric upraising and emplacement of upwelling mantle material (Koptev et al., 2015). This process has been influenced by the initial geometry of the lithosphere due to the presence of the thick Tanzanian craton, which diverted the upraising mantle towards the Eastern Branch where warm material accumulated at the base of the thinned lithosphere, increasing decompression melting

(Koptev et al., 2015). A general southward younging of the main volcanic phases (see Morley and Chantraprasert, 2022) is likely related to mantle plume dynamics (see below section 2.3).

2.3. Mantle plume(s) influence on rifting in the EARS

Rifting in East Africa has been attributed to the activity of one or more mantle plumes based on geophysical, geodynamical and geochemical evidences, as outlined hereafter.

2.3.1. Geophysical and geodynamical evidences for mantle plume activity

With the exception of the Turkana depression, the rift valleys of East Africa cut through broad elevated plateaus; this, together with the initial widespread flood basalt emplacement before significant rifting, has been related to mantle upwelling processes (e.g., Moucha and Forte, 2011; Hassan et al., 2020). The existence of one or several deep mantle plumes under the EARS is strongly supported by geophysical investigations, which have highlighted since a long time the occurrence of a large region of low velocity seismic waves rising from the core-mantle boundary, the so-called African superplume (e.g., Ritsema et al., 1999). However, the structure of the shallow mantle is not clearly defined by geophysical studies and the number and features of upwelling mantle domains remain debated (e.g., Boyce et al., 2021; Civiero et al. 2022 and references therein).

Irrespective of the number and structure of mantle plumes, upwelling of hot mantle material is believed to control rifting in the area. Africa and Somalia are indeed surrounded by oceanic ridges, and the plates are subjected to compression driven by ridge-push force, with no clear regional plate configuration to drive rifting (Coblentz and Sandiford, 1994). Rifting is instead related to extensional forces imposed by a combination of gravitational potential energy gradients related to mantle-driven uplift and basal drag from horizontal mantle flow at the base of the lithosphere (e.g., Stamps et al., 2014, 2015). The age-progressive volcanism in the EARS, characterised by an overall southward younging, has been interpreted as resulting from a southward migrating (Afar) plume relative to the African plate (e.g., Hassan et al., 2020; Morley and Chantraprasert, 2022).

2.3.2. Geochemical signature of plume material

A robust geochemical evidence for a deep mantle plume in the EARS derives from the occurrence of magmas with He isotopes >8 R_A (where R_A represent the He isotope composition of atmosphere, e.g., Halldórsson et al 2014; Castillo et al., 2020), which requires the predominant contribution of a deep undegassed mantle (e.g. Graham et al., 1992; 1998; Hanan and Graham, 1996). Additional evidence of anomalously hot rising mantle material is provided by the potential temperature recorded by olivine, which are in excess of >150 °C relative to the ambient upper mantle (e.g., Wong et al., 2022).

Many studies have tried to infer the geochemical and isotopic signature of this plume material from the magmatism of the northern EARS (e.g., Pik et al., 1999; Rogers et al., 2000; George and Rogers, 2002; Halldórsson et al 2014, 2022; Nelson et al 2012; Rooney et al., 2012; Furman et al., 2016; Castillo et al., 2020). The recent mafic magmas erupted at Erta Ale and Djibouti have been identified as representative of its composition or at least of its tail (e.g., Furman et al., 2016). This small range of values overlap with the postulated isotopic composition of the plume extrapolated by Rooney et al. (2012) from MER magmas ($^{87}Sr/^{86}Sr$~0.7035 and $^{143}Nd/^{144}Nd$~0.5129), similar to the composition of recent magmas of the Afar region (Castillo et al., 2020). Early flood basalts (HT2 basalts) of Ethiopia have been also considered a *proxy* for the composition of plume material (Kieffer et al., 2004; Muravyeva and Senin 2018) even though a contribution of the SCLM was proposed (Furman et al., 2016; Natali et al., 2016; Rooney, 2017; Nelson et al., 2019). In comparison with the previous compositions, the HT2 flood basalts have slightly more radiogenic $^{87}Sr/^{87}Sr$ (~0.7040) but similar $^{143}Nd/^{144}Nd$. In terms of Pb isotopes, the isotopic composition of the plume estimated by Rooney et al. (2012) and Castillo et al. (2020) are similar, with $^{206}Pb/^{204}Pb$~19.4-19.5 and $^{208}Pb/^{204}Pb$~39.2, while the HT2 flood basalts have less radiogenic Pb isotopic composition (Natali et al., 2016, Nelson et al., 2019). Finally, magmas from Kenya and Turkana have more radiogenic Pb isotopes and have been originally interpreted to reflect an additional HIMU component within the mantle plume (Furman et al., 2006) or a second mantle plume (George et al., 1998; Rogers et al., 2000), even though their Pb isotope signature was later considered to derive from the SCLM via drip melting (Furman et al., 2016).

Regarding the models accounting for the different age and geochemical heterogeneities of the early magmatism of the northern EARS, many interpretations have been proposed: from the existence of two different plumes (Afar and Kenya plumes, e.g., George et al., 1998; Rogers et al., 2000) to a single, chemically heterogeneous upwelling (Furman et al., 2006), or a hybrid model involving two branches of the same plume with different compositions (Nelson et al., 2012). According to the recent review by Rooney (2020d), the prevalent contribution of the deep mantle material beneath the EARS can be considered equivalent to a single plume, i.e. the Afar plume. Hereafter, we refer to the Afar plume to indicate the anomalous hot mantle beneath the EARS.

3. Sample selection and grouping

The full available database of the EARS magmas was downloaded from GEOROC (https://georoc.eu/) on 15th March 2021, selecting only the less evolved lavas (SiO_2 <52 wt%, MgO >4 wt%) to minimize the effects of crystal fractionation and crustal assimilation. The published data, consisting of more than 1500 samples, were implemented with new unpublished data from Ethiopia (25 samples) and the

Turkana depression (2 samples; Figure 1; Supplementary Table1). These new samples have been analysed for major, trace and Sr-Nd isotopes as detailed in the Supplementary Material.

All samples were then subdivided on the basis of temporal and spatial criteria based on the main tectonic and geodynamic evolution constraints along with the timing of magmatism as described above. Three main temporal periods were defined as follow (Figure 1):

i) 45-25 Ma, a time interval that defines the (pre-rift) flood basalt event;

ii) 25-10 Ma, an intermediate period characterised by time-space irregular initiation of deformation and heterogeneous volcanism (from continuation of flood basalt activity to more acid volcanism) among the Arabia, Nubian and Somalian plates;

iii) 10-0 Ma, the youngest interval related to the main rifting phases, with diffuse tectonic and volcanic activity.

From a spatial point of view, the samples were further subdivided into five different groups following the main tectonic domains of the EARS, roughly from N to S (Figure 1):

i) the Afar depression, which is characterised by incipient oceanic spreading and records the interaction;

ii) Ethiopia, which includes the Ethiopian rift valley and surrounding plateaux, characterised by significant tectono-magmatic activity in a lithosphere modified by magmatic processes;

iii) the Turkana depression, characterised by widespread tectonic and volcanic activity in a region of thinned crust following previous (Mesozoic) tectonic events;

iv) the Eastern Branch, where an intense volcanic activity is generated due to warm material accumulated at the base of a thinning lithosphere;

v) the Western Branch, which has a limited extension and forms narrow, deep basins and localised volcanism in a region of cold and strong lithosphere.

In order to correctly understand our final interpretation of the analysed data, it is important to bear in mind that the distribution of samples of the selected database does not actually represent the distribution of the volcanic products in nature, on both volumetric and temporal basis. As an example, the samples from the recent period (10-0 Ma) in the Western Branch are as abundant as the ones from the Eastern Branch, whereas the volumes of erupted magmas from the latter area are much larger than those from the former region. Also, not all different magmas have been retrieved for their isotopic composition, limiting the completeness and the representativeness of our database. For example, no isotopic analysis on samples from the Western Branch older 10 Ma are available, despite limited volcanism has occurred in the area since ~25-26 Ma (Figure 1). Nevertheless, our database may be considered well representative for our purpose: from a spatial point of view, all the selected samples

are evenly distributed within the main volcanic regions. The temporal distribution of samples is in line with the overall southward younging of volcanism described above: consequently, the oldest interval is sampled in the northern areas only (Afar, Ethiopia, Turkana), whereas progressively younger volcanic rocks are sampled moving southwards (Eastern Branch and Western Branch). In detail, most of the selected samples are from the recent (10-0 Ma) volcanic activity (Afar 19%, Ethiopia 13%, Turkana 2%, Eastern Branch 23%, Western Branch 24%) although magmas from the other two periods of activity in the different areas are represented as well (19% in total) with the exception of the Eastern Branch and Western Branch having no samples with an emplacement age >25 Ma and >10 Ma, respectively.

4. Geochemical characteristics of mafic magmas

The chemical composition of mafic magmas varies from basalt, picrobasalt, trachybasalt, basanite and foidite with the Eastern and Western Branch samples having the most undersaturated compositions. All the selected samples, but the magmas from the Eastern and Western Branches, have a relatively constant CaO/Al_2O_3 with decreasing MgO (Figure 2) in agreement with the compositional variation of mantle-derived magmas from oceanic areas (MORB and OIB; GEOROC database). This signature provides evidence for the reliability of the screened samples in terms of minimising geochemical variations due to low-pressure fractionation processes. Figure 2 shows that olivine is the main mineral responsible for the observed decrease in MgO. Admittedly, at MgO <7% a subset of samples have a combined decrease in MgO and CaO/Al_2O_3, suggesting an additional minor role of clinopyroxene fractionation. The effect of clinopyroxene fractionation could be removed by limiting the database to samples with MgO >7% but, since we will mostly discuss variations in incompatible trace elements that are negligibly affected by clinopyroxene and olivine, we decided not to restrict the database. The magmas from the Eastern and Western Branches have higher CaO/Al_2O_3 than other EARS magmas (Figure 2), demanding for an origin from different mantle source domains, which will be considered in the following sections.

Another useful comparison between our EARS samples and MORBs and OIBs is reported in the Th/Yb *vs.* Ta/Yb diagram (Figure 3). Most the mafic magmas of the older two periods of activity are superimposed to OIB compositions and denote a provenance from fertile mantle sources. Half of the samples from Ethiopia have, however, lower Ta/Yb and Th/Yb indicating either an origin from more depleted mantle sources (Pik et al., 1999) or higher mantle melting degrees, as suggested by their high MgO contents (MgO>10 wt.%, Figure 2a). The latter hypothesis comes from the observation that the degree of incompatibility during mantle melting increases from Th to Ta and Yb (e.g., Sun and McDonough, 1989; McKenzie and O'Nions, 1991; Kelemen et al., 2003), meaning that, starting

from the same mantle source, the higher the melting degree, the lower Th/Yb and Ta/Yb in produced melts. Most mafic magmas of the youngest period of activity (Figure 3b) cluster at similar Th/Yb and Ta/Yb as the older mafic magmas, except samples from the Eastern and Western Branches, which show higher Ta/Yb and Th/Yb. This characteristic requires the contribution of other mantle source domains as also attested by their high CaO/Al_2O_3 (Figure 2b). The Afar samples with low Th/Yb and Ta/Yb (Figure 3a) recall a depleted mantle sources as suggested for the Ethiopia mafic magmas of the oldest period of activity (Barrat et al., 2003; Daoud et al., 2010).

4.1. Partial melting of the mantle source

Constraints on the depth and degrees of mantle melting originating the EARS mafic magmas can be assessed by Rare Earth Element (REE) fractionation. One of the most useful diagrams is Yb *vs.* La/Yb, which is strongly dependent upon mantle melting in the garnet and spinel stability fields. We have modelled the REE signature of the EARS mafic magmas (Figure 4) applying a non-modal batch melting to a nominal Primitive Mantle (McDonough and Sun, 1995) and SCLM (McDonough, 1990) using partition coefficients from the compilation of McKenzie and O'Nions, (1991) and Kelemen et al. (2003). Both sources are not meant to be the actual mantle domains of the overall EARS mafic magmas; rather, they are used as *proxies* to have a qualitative information on melting degrees and depths (e.g. Ayalew et al., 2018; Feyssa et al., 2019; Tortelli et al., 2022).

The REE fractionation of mafic magmas belonging to the oldest two periods of activity (Figure 4a) are consistent with variable melting degrees of a primitive mantle source both in the garnet and spinel stability fields, with a few samples from Ethiopia, Turkana, and Eastern branch indicating lower degrees of mantle melting (<1%) predominantly in the garnet stability field. In contrast, the EARS mafic magmas of the youngest period of activity reveal a significant dichotomy. The Afar, Turkana, and Ethiopia samples suggest an origin from variable melting degrees of a primitive mantle source almost entirely in the spinel stability field (Figure 4b**)**, whilst the Western Branch and, to a lesser extent, the Eastern Branch samples have extreme La/Yb values (up to 320), which are not consistent with melting of a primitive mantle-like garnet lherzolite (Figure 4b) even at very low melting degrees. Their REE fractionation fits better with an origin from a SCLM source in the garnet and spinel stability fields at low melting degrees (Figure 4c).

4.2. Mantle source mineralogy

Incompatible trace element ratios can provide constraints on minor mineral phases occurring in the mantle source in addition to a *normal* lherzolite (olivine + orthopyroxene + clinopyroxene ± spinel ± garnet). Ba/Rb *vs.* Rb/Sr yields information on the role of K-bearing phases in the mantle source (e.g.,

Furman and Graham, 1999). Deviations from primitive mantle and SCLM estimates indicate metasomatic enrichment events: mantle-derived magmas in equilibrium with phlogopite-bearing lherzolite are expected to have significantly higher Rb/Sr and lower Ba/Rb than those in equilibrium with amphibole-bearing lherzolite (Figure 5). The EARS mafic magmas of the older two periods of activity cluster from primitive mantle composition towards high Ba/Rb in the case of Ethiopia and Turkana mafic magmas (Figure 5a), suggesting an origin from a lherzolite variably metasomatised by amphibole. In contrast, a few samples from Ethiopia, and the Western and Eastern Branches have high Rb/Sr pointing to a phlogopite-bearing mantle source. Mafic magmas of the youngest period of activity show a more pronounced affinity for a lherzolite variably metasomatised by amphibole and/or phlogopite (Figure 5b). Phlogopite-bearing lherzolite melts are prevalent, albeit not exclusively, in the Western and Eastern Branches mafic magmas (Foley et al., 2012, Rosenthal et al., 2009), whilst amphibole-bearing lherzolite melts are more abundant in the Eastern Branch, Turkana, Ethiopia, and Afar mafic magmas. The presence of phlogopite in the mantle beneath the EARS is supported by the occurrence of phlogopite-bearing mantle xenoliths, which are common in the northern sector of the Western Branch (Foley et al., 2012, Lloyd et al., 2002). In the Western Branch, the presence of phlogopite and mantle melting at depth > 100 km is also attested by the occurrence of kamafugites (and possibly kimberlites) (Foley et al., 2012, Tappe et al., 2020).

In addition to phlogopite and amphibole, the trace element signature of EARS mafic magmas reveals another minor component likely occurring in their mantle source. This is displayed by Zr/Nb *vs.* Nb/Ta (Figure 6). Zr/Nb is fractionated during mantle melting and represents a *proxy* of source fertility, with MORBs having higher Zr/Nb than OIBs because the former originate from more depleted mantle domains. In contrast, Nb and Ta have similar partition coefficients during mantle melting, as attested by the rather constant Nb/Ta in MORBs and OIBs (Figure 6). The EARS mafic magmas of the older two periods of activity suggest an origin from a variable depleted/enriched mantle source (2<Zr/Nb<40), similar to MORBs and OIBs, and without any significant Nb/Ta fractionation (Figure 6a). Admittedly, most samples are from the Ethiopia albeit a few samples are also from Turkana and Eastern Branch. As with other trace element ratios, the EARS mafic magmas of the youngest period of activity display differences with respect to the oldest mafic magmas (Figure 6b). While most of Afar, Ethiopia, and Turkana mafic magmas plots within the range defined by the oldest lavas and oceanic area basalts, some samples from the Eastern and Western Branches are displaced toward higher Nb/Ta (up to ca. 50), with the latter shifting also towards low Zr/Nb values (down to <1). This peculiar signature suggests carbonatitic metasomatism of the mantle source (Green, 1995; Pfänder et al., 2012; Bragagni et al., 2022) and can also explain their high CaO/Al_2O_3 (Figure 2 and Foley et al., 2012). Carbonatites are indeed widespread in these two regions (e.g., van

Straaten and Bell, 1989; Bell and Blenkinsop, 1987; Foley et al., 2012; Guzmics et al., 2019) and possess the unique Nb/Ta and Zr/Nb signature (Hoernle et al., 2002; Bizimis et al., 2003; Chakhmouradian, 2006) required to explain the offset of the Eastern and Western Branch magmas from typical values of oceanic (MORBs, OIBs) and continental (e.g., other EARS) mafic magmas. Overall, the trace element characteristics of the EARS mafic magmas are roughly consistent with a progressive increase of the contribution of metasomatic mantle sources, especially in the southern part of the rift and in the youngest volcanic activity.

4.3. Radiogenic isotopes

Radiogenic isotope compositions of EARS mafic magmas are reported in Figure 7 along with fields of MORBs and OIBs. The Afar and Ethiopia mafic magmas of the older two periods of volcanic activity (Figure 7a) cluster around the composition that is considered to represent the Afar mantle plume (Rogers et al., 2000; George and Rogers, 2002; Rooney et al., 2012; Castillo et al., 2020) with trends towards the MORB, EM I, and EM II mantle components of the mantle zoo (e.g., Hofmann, 1997; Stracke and Hofmann, 2005). The Turkana and a subset of the Ethiopia samples are displaced towards a HIMU component suggesting, following some interpretations, the occurrence of a different plume (i.e., the so-called Kenya plume, Rogers et al., 2000). The Eastern Branch samples are displaced from the Afar and the putative Kenya plume to less radiogenic Nd isotope compositions and also display a trend towards radiogenic Sr isotope compositions ($^{87}Sr/^{86}Sr$ up to 0.706), which is offset from the EM II mantle component (Figure 7a).

In contrast, the EARS mafic magmas of the youngest period of activity have a widespread range of isotopic compositions starting from the Afar mantle plume to the MORB-like mantle and to extremely radiogenic Sr isotope and unradiogenic Nd isotope compositions, far exceeding the EM II and EM I mantle components (Hofmann, 1997), respectively (Figure 7b). The Afar mantle plume component is present, with no exception, in all of the mafic magmas of this period, whilst the radiogenic Sr isotope mantle component is predominant in the Western Branch mafic magmas, with a few samples from the Eastern Branch, in agreement with the contribution of a phlogopite-bearing lherzolite (Figure 5). The unradiogenic Nd isotope mantle component is restricted to the Eastern Branch mafic magmas and is even more extreme than that of the previous periods of activity (Figure 7), requiring a low time-integrated Sm/Nd.

Lead isotope compositions of EARS mafic magmas have less, albeit significant, differences between the oldest and youngest periods of volcanic activity (Figure 8). As with Sr and Nd isotopes (Figure 7), the samples, starting from the common Afar plume component, are offset towards MORB, EM I, EM II, and HIMU mantle components. Most of mafic magmas are aligned along the NHRL defined

by MORBs and OIBs, with Afar, Ethiopia, and Turkana mafic magmas having generally less radiogenic Pb isotope compositions than those of the Western and Eastern Branches (Figure 8). In particular, the recent Western Branch mafic magmas deviates from the other EARS magmas, pointing towards more radiogenic $^{207}Pb/^{204}Pb$ at the same $^{206}Pb/^{204}Pb$ (Figure 8b). Such a radiogenic $^{207}Pb/^{204}Pb$ signature exceeds the range observed in magmas with EM II affinity, requiring the contribution of an old crustal component with high time-integrated U/Pb. Instead, the Eastern Branch mafic magmas of the three periods of activity are offset towards HIMU-like compositions (Figure 8). Such a shift to a HIMU mantle component is odd with their extreme unradiogenic Nd isotope composition (Figure 7b). Another peculiar characteristic is that the Turkana and the subset of the Ethiopia samples, although suggesting the occurrence of a HIMU mantle component in the Sr-Nd isotope diagram (Figure 7a), do not have Pb isotope compositions recalling the HIMU mantle component (Figure 8).

As with trace element ratios (Figures 3-6), Sr-Nd-Pb isotope compositions of the EARS mafic magmas reveal significant spatial and temporal variations and allow to place important constraints on the contribution of different mantle domains in magma genesis during the evolution of the rift. In particular, since there is geochemical evidence for the influence of the SCLM in the magmatism of the EARS (e.g. Furman et al., 2016), in addition to the Afar mantle plume, we will focus on the role of the SCLM in affecting the isotopic signature of magmas in space and time. The geochemical and isotopic compositions of mantle xenoliths from different lithospheric African domains provides the opportunity to assess their role in the EARS magmatism.

5. The message from the radiogenic isotope signature of mantle xenoliths

In order to investigate the contribution of the SCLM on magma genesis, we collected available radiogenic isotope data (Sr-Nd-Pb-Os) on ultramafic mantle xenoliths (GEOROC database) that are representative of SCLM fragments sampled by ascending magmas of the EARS and the surrounding regions (Arabia peninsula and South Africa). These data are compared with the observed trends in the EARS mafic magmas to constrain their genesis in space and time at the scale of the whole rift system.

5.1. Sm-Nd isotope composition

The Sm-Nd isotope systematics can be successfully used to retrieve age information on ultramafic garnet-bearing rocks. In the Sm-Nd isochron diagram (Figure 9), the ultramafic xenoliths are roughly distributed along two different trends, revealing two distinct formation ages of the African SCLM. The reference isochrons reported in Figure 9 were calculated starting from the Nd isotope

composition of either the primitive (dashed lines) or the depleted mantle (solid lines). The most recent reference isochrons comprise most of the mantle xenoliths and are consistent with a relatively young event at ~600 Ma. This age, recorded by fragments of the SCLM, includes samples from the African continent (South Africa, Tanzania, Ethiopia) and Arabia (Figure 9). The other reference isochrons encompass samples from the Tanzanian craton and record an older event at ~2.6 Ga. These two pairs of reference isochrons are consistent with the two main formation events of the SCLM during the Archean and the Pan-African (Chesley et al., 1999, Burton et al., 2000).

Finally, carbonatites occurring in the southern portion of the EARS (both Western and Eastern Branches) are incidentally broadly aligned along both the Pan-African and Archean reference isochrons (Figure 9) suggesting an origin from a metasomatised SCLM (Foley et al., 2012).

5.2. Os isotope composition

The Re-Os isotope systematic provide further age constrains on events recorded by mantle xenoliths. Since Re is incompatible and Os is compatible during mantle melting, the Os isotope signature of the mantle is "frozen" after melt extraction. As such, the so-called Re-depletion model ages (T_{RD}) represent a tool to date the formation of the lithospheric mantle (Walker et al. 1989). Importantly, metasomatic events in the SCLM can overprint the original Re-Os isotopic signature, making T_{RD} ages only reliable "minimum ages". If metasomatism acts in an unsystematic way, information can be still obtained when considering the distribution of T_{RD} ages. A survey of T_{RD} Os ages from mantle xenoliths of the EARS shows three main peaks at ca. 2.8, 1.5, and 0.5 Ga (Figure 10). The T_{RD} ages are all calculated using the primitive mantle estimates of Meisel et al. (2001) and might slightly differ from those reported in the original publications, where different reference reservoirs had been used. Despite the limited number of data, the three T_{RD} age peaks are also observed in mantle xenoliths from individual volcanic centres.

In north Ethiopia, near the Afar depression, most T_{RD} ages are clustered around 0.6 Ga. Even if these model ages were originally interpreted as "disturbed" with no age meaning (Alemayehu et al., 2019), it is striking that they define a relative narrow range, matching the Pan-African event. Although limited to only two samples, older T_{RD} ages of 1.6 and 1.2 Ga, points to portions of the lithosphere that was Archean in age and later (partially) overprinted (Alemayehu et al., 2019). Mantle xenoliths from the northern Turkana depression show a rough bimodal T_{RD} age distribution with a first peak around 500 Ma and an older asymmetric peak at 1.5 Ga, which includes T_{RD} ages up to 2.4 Ga. The oldest T_{RD} ages of the EARS (up to 3.4 Ga) are recorded in mantle xenoliths from the Eastern Branch (Burton et al., 2000; Chesley et al., 1999; Meisel et al., 2001) with a clear Archean signature, resulting in a main peak at around 2.6 Ga. This ancient signature is consistent with the formation of the

Tanzanian craton at 2.8-3.4 Ga (Chesley et al., 1999; Burton et al., 2000). Unfortunately, no T_{RD} ages are available for mantle xenoliths from the Western Branch of the EARS.

The three T_{RD} age peaks observed in the complete dataset of the EARS, reflect also variable contribution of different lithospheric domains. In particular, Archean T_{RD} ages are recorded only around the Tanzania Craton, while Pan-African ages are mostly recorded in the north, near the Afar region. These ages are consistent with what observed with Sm-Nd isotopes (Figure 9), stressing the importance of two lithospheric mantle domains, affected by (at least) two distinct events. The additional peak at 1.5 Ga, recoded by the samples from northern Turkana depression in the T_{RD} density probability plot (Figure 10) could reflect a rejuvenation of the Archean lithosphere (i.e., no age meaning) or express an additional event in the lithospheric mantle. Following the second possibility, a 1.5 Ga geological event was proposed by Alemayehu et al. (2019) on the basis of a linear array of xenoliths in a Re-Os isochron diagram. The regression through these data yielded a 1.5 Ga age, synchronous with the break-up of the Nuna supercontinent (Alemayehu et al., 2019). Although the error on the inferred initial Os isotopes is large ($^{187}Os/^{188}Os = 0.117\pm0.003$, Alemayehu et al., 2019), it is consistent with the composition of the primitive mantle at that time ($^{187}Os/^{188}Os$ = 0.118), possibly reflecting the formation of specific domains of the lithospheric mantle at that time as also suggested by the peak in the T_{RD} ages.

Despite the strong evidence of metasomatism in many mantle xenoliths of the EARS, which is expected to affect the Os isotope signature (Chesley et al., 1999; Burton et al., 2000; Reisberg et al., 2004; Alemayehu et al., 2019), it is surprisingly that whole rock T_{RD} ages are able to preserve age information. For instance, a positive correlation between $^{187}Os/^{188}Os$ and $^{187}Re/^{188}Os$ (Chesley et al., 1999, Burton et al., 2000, Reisberg et al., 2004) is inconsistent with a "frozen" Os isotopic signature after melt extraction. Similarly, the inverse correlation between $^{187}Os/^{188}Os$ and indices of melt depletion (e.g., Al_2O_3, Lu, CaO) can be explained by incomplete extraction of Re after partial melting, which is however at odd with what expected after large degrees of partial melting required for the formation of highly refractory cratonic mantle roots. This points towards metasomatic event that introduced radiogenic Os along with Al_2O_3, Lu, CaO and Re (e.g., Chesley et al., 1999; Reisberg et al., 2004). The fact that these correlations are not ubiquitously observed could reflect a limited metasomatic influence on T_{RD} ages, thus affecting only few samples. Moreover, Re-enrichment, which is characteristic of melt/fluid infiltrations shortly before or during the eruption of the magma hosting the xenolith (e.g., Chesley et al., 1999), does not have a large effect on the Os isotope composition when the eruption is relatively recent. More speculative scenarios to explain the occurrence of primary Os isotope signatures in mantle domains affected by metasomatism include Os mobility within the mantle in the form of sulfide melts (Reisberg et al., 2004). Thus, through

migration of sulfide melts, the Os isotopic composition could be transferred from its original mantle domain to other ones without being significantly affected and, therefore, reflecting the formation of residual mantle domains (Bragagni et al., 2017).

6. Mantle domains involved in the genesis of rift-related volcanism

The geochemical features of EARS mafic magmas strongly depend on the interaction and mixing between a common deep plume-derived material and other mantle domains (e.g., Rooney, 2020d and references therein). A depleted asthenospheric component (DMM), which is clearly observed in the magmatism of the Gulf of Aden and Red Sea (e.g. Altherr et al., 1990), is likely involved in some of the magmatism of the EARS. Indeed, the contribution from DMM can explain the low Th/Yb e Ta/Yb (Figure 3) and the radiogenic Nd isotope composition (Figure 7) of the first products of Ethiopia magmas (Pik et al., 1999; Kieffer et al., 2004) and some of the younger Afar magmas (Barrat et al., 2003, Daoud et al., 2010). Similarly, a DMM involvement is also invoked in the Turkana area (Furman et al., 2006, Figure 7). As such, a variable contribution of a depleted mantle to the inferred Afar plume composition can explain the isotope variability towards high $^{143}Nd/^{144}Nd$ and low $^{87}Sr/^{86}Sr$. However, the largest variations in Sr-Nd-Pb isotopes in the EARS magmas, roughly defining two trends, one with radiogenic $^{87}Sr/^{86}Sr$ (exceeding the oceanic EMII end-member) and moderately unradiogenic $^{143}Nd/^{144}Nd$, and the other with extremely unradiogenic $^{143}Nd/^{144}Nd$ and moderately low $^{87}Sr/^{86}Sr$ (Figure 7), point towards the involvement of others contributions from different mantle end-members such as the SCLM.

The contribution of the SCLM to magma genesis in the EARS might be extremely complex and variable (e.g., Furman and Graham 1999, Rosenthal et al., 2009; Foley et al 2012; Rooney, 2020d), although its role seems widespread and ubiquitous, as already observed in Ethiopia (e.g. Natali et al 2016; Feyissa et al 2017, 2019; Beccaluva et al 2009; Rooney, 2017), Western Branch (e.g., Spath 2001, Rosenthal et al 2009; Furman and Graham 1999), Eastern Branch (e.g, Rogers, 2006), and Turkana (e.g. Meshesha et al 2011; Furman et al 2016). The Sr-Nd isotope signature of mantle xenoliths (Figure 11) can help to understand the link between SCLM and the EARS mafic magmas. In the same diagram, the isotope compositions of carbonatites from this area are also reported, as these magmas are thought to derive from strongly metasomatised SCLM sources (e.g. Foley et al., 2012; Rooney, 2017; Rooney 2020d). It is striking to observe that the isotopic signature of the mafic magmas nicely overlap with that of mantle xenoliths and carbonatites. Notably, mantle xenoliths points to even more extreme compositions (Figure 11). Since the isotopic composition of the mantle xenoliths are consistent with two events (Archean and Pan-African, section 5.1), the two trends in the Sr-Nd space observed in EARS magmas can be ascribed to the interaction of the Afar mantle plume

with these two different SCLM domains. In this scenario, magmas trending towards extremely radiogenic $^{87}Sr/^{86}Sr$ and moderately unradiogenic $^{143}Nd/^{144}Nd$ are affected by the Pan-African SCLM (Mobile Belt of Rooney, 2020b), while magmas pointing towards very low $^{143}Nd/^{144}Nd$ show an affinity with the Archean lithosphere (Craton of Rooney, 2020c). Although there are several lines of evidence that the SCLM experienced multiple events and types of metasomatism (e.g., Rosenthal et al., 2009; Rooney 2020d), its Sr-Nd isotope signature is roughly consistent with these two components, at least at the very large scale of Figure 7.

The extreme radiogenic isotope compositions recorded in the Western and Eastern Branches can be therefore obtained by admixing the Afar mantle plume with the two different domains of the SCLM (Pan-African and Archean) as recorded by ultramafic mantle xenoliths (Figures 7, 8, 11). In this scenario, the trend observed in the older magmas of the Eastern Branch can be explained by a contribution of both SCLM domains: the interaction with the Archean lithosphere can result in the general lower $^{143}Nd/^{144}Nd$ of these magmas than those of the Afar mantle plume, while the Pan-African lithosphere can be responsible for the trend towards high $^{87}Sr/^{86}Sr$ with only a moderate decrease in $^{143}Nd/^{144}Nd$ (Figures 7a, 11a). Most of the younger samples, with extreme unradiogenic Nd isotope compositions, point towards a stronger contribution from the Archean SCLM, whereas the remaining samples, with radiogenic Sr isotope compositions, indicate the contribution of the Pan-African SCLM (Figures 7b, 11a). Notably, the samples of the Eastern Branch with the strongest Archean signature are from volcanic centres located within the Tanzania craton, while the Pan-African signature is recorded in samples from the Mozambique mobile belt along the craton boundary. Overall, there is a trend of increasing contributions with time of SCLM domains to magma genesis (see below).

The Western Branch, where only samples from the youngest period of volcanic activity are available, shows a more uniform trend towards the Pan-African lithosphere, reaching the most extreme radiogenic Sr isotope compositions (Figures 7b and 11a). Many studies highlighted the complexity of the different metasomatic processes, involving a significant role of silicate and carbonatitic melts in the SCLM of the Western Branch (Furman and Graham, 1999; Foley et., 2012; Rosenthal et al., 2009). However, from the large scale of Figure 7, the isotopic composition of the Western Branch magmas spreads along a rather distinct trend, dominated by Pan-African SCLM, suggesting that the overall metasomatism within the Western Branch mimics this general trend. Furman and Graham (1999) identified a common lithospheric mantle (CLM) with a composition of $^{87}Sr/^{86}Sr = 0.7050$ and $^{143}Nd/^{144}Nd = 0.51264$, which falls within our Pan-African trend, although not reaching the extreme radiogenic Sr isotopes observed in the Western Branch magmas (Figure 7).

The observed temporal and spatial variations based on Sr and Nd isotopes are also consistent with what observed on Pb isotopes (Figures 8, 11b). The spread towards radiogenic Pb isotopes observed especially in the Eastern Branch samples are consistent with a SCLM contribution that was enriched in carbonatite-like domains characterised by high time-integrated U/Pb (Figure 11b). Such a component can be observed both in ultramafic mantle xenoliths and in carbonatite magmas (Figure 11b). This extreme radiogenic Pb isotope signature points towards a HIMU-like mantle component. Such a component was previously interpreted to potentially reflect an additional mantle plume or a distinct portion of the African Superplume (e.g., Rooney 2020d for a review on the topic). In particular, the HIMU plume component was proposed for the Turkana and South Ethiopia areas (the Kenya plume, Rogers et al., 2000), possibly reflecting the deep recycling in the mantle of about 30% ancient (1.7–2 Ga) hydrothermally altered subducted oceanic crust (Furman et al., 2006, Nelson et al., 2012). The Turkana and South Ethiopia magmas, however, do not have the Pb isotope signature of HIMU basalts as displayed by the Eastern Branch magmas (Figures 8). This suggests that the HIMU signature, coupled with extreme Sr-Nd isotope compositions (Figures 11a), can be obtained with carbonatite metasomatism (Figures 11a), which is well known to affect portions of the local SCLM (e.g., Rooney et al., 2014; Muirhead et al., 2020). The $^{187}Os/^{188}Os$ of Turkana magmas are slightly more radiogenic than the inferred composition of the Afar mantle plume, which could reflect deep recycling of oceanic crust (Nelson et al., 2012) but also a similar component in the local SCLM. Indeed, metasomatism can enrich the SCLM in Re as attested, for example, by the radiogenic $^{187}Os/^{188}Os$ of eclogite and pyroxenites from cratonic settings (e.g., Aulbach et al., 2009). As such our interpretation may also support an origin of the HIMU signature in the SCLM by metasomatism or dripping (Rooney et al., 2014; Furman et al., 2016). Whatever the name of this signature, the important aspect is that chemical and isotopic variations of the EARS magmas require that the SCLM was affected by mantle metasomatism (e.g., Rooney, 2020d; Furman 2007), which is best observed in Pb isotopes (likely in the form of carbonatite metasomatism), but that does not seem to have fully overprinted the Sr-Nd-Os isotope signature inherited from the Archean and Pan-African events. Interestingly, based on Pb isotopes, a metasomatic age of ca. 500 Ma (i.e., Pan-African) was proposed for the source of the Western Branch (Vollmer and Norry 1983) along with an older event of ca. 1 Ga (Rogers et al., 1998).

A slightly different mechanism is required to explain the Pb isotope composition of the Western Branch magmas, pointing to an EM II-like mantle component (Figure 8). This signature, coupled with their Sr-Nd isotope composition (Figure 7), requires the contribution of an old crustal component in the SCLM (e.g., Furman et al., 2007; Castillo et al., 2014), likely referred to the Pan-African event (Figures 9, 11).

In summary, the radiogenic isotope signature of the SCLM, as recorded by mantle xenoliths and carbonatites, covers the whole compositional range observed in EARS mafic magmas. Although the picture might be more complex when considering the variable chemical composition of metasomatic melts/fluids and their impact on the small-scale chemical variations of the EARS magmas (e.g., Furman et al., 2016; Rooney 2020d), our findings highlight that the SCLM contains the geochemical signature required to explain the large variations observed in the EARS magmatism throughout the interaction with the Afar mantle plume and to a lesser extent the DMM asthenospheric mantle.

6.1. Mechanism for the contribution of the SCLM in the EARS magmas

The SCLM, which comprises an old Archean domain and a more recent Pan-African component, plays a crucial role in the genesis of the EARS magmas and their geochemical fingerprints. Another important outcome of our analysis is that, at large-scale, the SCLM contribution seems to increase with time, as magmas of the third younger period of activity (<10 Ma) show the more extreme isotopic variation.

Melt production from the SCLM is, however, paradoxical because it is much colder than the convective asthenosphere, and it should be highly depleted in those major elements necessary for basalt generation (e.g., Arndt and Christensen, 1992). Enrichment processes involving percolation of silicate melts and volatile-rich fluids have been, however, proposed to explain re-fertilisation and melting of the SCLM at temperatures below the solidus of dry peridotite (e.g., Hawkesworth et al., 1984; Menzies and Hawkesworth, 1987; Stolz and Davies, 1988; Ionov et al., 2002). Other factors including extension rate, lateral temperature gradients, inputs of external heat by mantle plumes impinging and flattening at the base of the lithosphere may also contribute to SCLM melting (e.g., McKenzie and Bickle, 1988).

In the case of the EARS, re-fertilisation of the SCLM likely occurred during the Archean and Pan-African events (Figure 9) and different mechanisms for explaining SCLM melting have been proposed. The arrival of the hot plume material at the base of the lithosphere could provide the heat necessary to trigger melting at the base of the lithosphere (e.g., Rogers et al., 1998; Beccaluva et al., 2009), especially in easily fusible metasomatic portions (Steiner et al., 2022). Alternatively, portions of the bottom of the lithosphere could be physically transported through later advection into a region of melting near the boundary of thick lithospheric domains such as those expected at the margin of cratons (Muirhead et al., 2020). Another possibility is represented by drip melting, which requires metasomatised lithospheric portions that first sink into the asthenosphere due to their higher density and then melt (Furman et al., 2016). Geochemically it is difficult to discriminate between these

different scenarios, but it is possible to do some considerations according to the time variations in the magmatism as discussed in previous sections.

The scenario we propose is represented by initial plume arrival with uplift and volcanism in the absence of significant extension (e.g., Corti, 2009). In these conditions, the interaction between the uprising plume and the lithosphere is limited, with the lithosphere being too cold to melt. Instead, in the rigid lithosphere, the development of throughgoing fractures and faults during plume-related uplift facilitates direct transport of mantle melts *en route* to the surface (Figures 7, 8; e.g., Beccaluva et al., 2009). This well explains the predominance of the plume component in the initial melts (40-25 Ma and 25-10 Ma), a scenario which is appropriate for Afar, Ethiopia and Turkana (Figures 7, 8). The minor SCLM signature in these magmas may be related to local melting of limited portions of the lithosphere in response to an increase of the geothermal gradient related to the arrival of the plume (e.g., Beccaluva et al., 2009). Successively, due to the continued spreading of the plume head beneath the plate and the continued heating of the lithosphere, the SCLM overpassed the solidus and started to contribute significantly to melt production. This process was further enhanced in the youngest period of volcanic activity (10-0 Ma) by the onset of the main rifting phases, with progressive thinning of the lithosphere and progressively shallower melting. In this phase, the increase in the SLCM component may be also enhanced by an overall progressive weakening of the upraising plume and a relative motion of the plume head away from Ethiopia, Afar and the Turkana depression (Hassan et al., 2020). This process therefore may explain the overall large-scale increase of the SCLM-like signature (Archean and Pan-African) in the recent EARS magmas (10-0 Ma, Figures 7, 8).

It is worth noting, however, that the picture may be more complex and apparently contradictory at a smaller temporal and spatial scale. For instance, the isotopic signature in the most recent magmatism of the Turkana and Afar regions (< 2 Ma) points to that of the Afar plume (Furman et al., 2006), with an absence of SCLM. In the case of the Afar, the lack of SCLM signature in the recent magmas is readily explained by the extremely thin or absent lithospheric mantle of the area (e.g., Rychert et al., 2012), which is close to a phase of oceanisation (e.g., Bastow and Keir, 2011). For the Turkana depression, the waning of the SCLM component might be related to vanishing of an episode of drip melting (Furman et al., 2016). Similarly, also the locally thin lithosphere in portions of the Western Branch was interpreted as due to drip melting and the variation in Sr-Nd isotope composition as a consequence of removal of the lower portions of a layered lithosphere (Lawrence et al., 2022).

7. Summary: spatial and temporal variations in magma production through the EARS

The scenario of magma production along the EARS obtained from our critical analysis of the available geochemical data of mafic magmas and mantle xenoliths from different sectors of the rift,

integrated with new trace element and Sr-Nd isotope data from the Main Ethiopian Rift and Turkana depression, is summarised and illustrated in Figure 12. It is important to remark here that the distribution of samples in our database does not represent, from both volumetric and temporal points of view, the actual distribution of the volcanic products (see paragraph 3). Despite these limitations, our database is fully representative and our analysis offers a geochemical picture which is consistent with previous investigations of magma production in the EARS (e.g., Rooney, 2020d and reference therein) and allows additional constraints on these processes.

In the time interval between 45 and 25 Ma (Figure 12a) volcanic activity was limited to Ethiopia, Afar and the Turkana tectonic domains, affected by impingement of the upraising mantle plume which caused volcanism and plateau uplift well before the main rifting episodes. Consequently, magmas from this older phase mainly involved a plume component with minor contributions from the SCLM (Archean domain in the Turkana depression and Pan-African domain in Afar and Ethiopia) and the DMM.

In the second time interval (25-10 Ma), the DMM component disappeared in both the Afar and Ethiopia, whereas it was still involved in the magma genesis of the Turkana depression which did not significantly change its signature with respect to the first period of volcanism (Figure 12b). The available data from the Eastern Branch indicate the presence of a mantle plume component associated with variable contributions from the SCLM in both its Archean and Pan-African domains (Figure 12b).

The youngest period of volcanic activity (10-0 Ma) corresponds to the main rifting phases all along the EARS (Figure 12c): widespread volcanism still records a significant contribution from the upraising plume material and an increasing signature of the Archean and Pan-African SCLM domains. Specifically, the Archean SCLM contributed to the magmatism of the Eastern Branch, where rifting propagated within the Tanzanian craton, while the Pan-African SCLM influenced the magmatism outside the craton along the Pan-African mobile belts in both the Eastern and Western Branches. Carbonatite magmas as well, which might have been generated directly within the carbon-rich Tanzanian lithospheric mantle (Eggler and Bell, 1989) or through liquid immiscibility from silicate melts (Brooker and Kjarsgaard, 2011), contributed to the geochemical signature of the Eastern and Western mafic magmas of the EARS (Figures 6, 11b).

Overall, our critical analysis of the screened database indicates that the trace element and radiogenic isotope signatures of the EARS mafic magmas are fully consistent with a relatively homogenous, single mantle plume (Rogers et al., 2000; George and Rogers, 2002; Rooney et al., 2012; Castillo et al., 2020) which is variably contaminated, depending on temporal and spatial distribution (Figure 12), by different Archean and Pan-African SCLM domains (phlogopite- and amphibole-bearing

metasomatised peridotites) plus a depleted asthenospheric component (DMM). The plume contribution in the volcanism of the Eastern Branch starting at 25 Ma, and of the Western Branch starting at 10 Ma is consistent with the model invoking a single Afar plume migrating southwards relative to the African plate (Hassan et al., 2020). The increasing contribution of the different SCLM domains is related to the main rifting phases especially in Ethiopia and Eastern and Western Branches, in which extensional processes have progressively allowed melting of the SCLM. In this view and at our scale, a simple increasing of lithosphere melting, provides the simplest mechanism to explain the overall variability with time without the need to evoke other complex models involving the occurrence of multiple mantle plumes.

Acknowledgments

We thank Sebastian Tappe and an anonymous Reviewer for the detailed, constructive comments which helped to significantly improve this manuscript. Derek Keir and Federico Sani are thanked for discussions and suggestions. We also thank Daniele Maestrelli for the help on the location of samples in Figure 1. This research has been partly funded by MiUR project PRIN2017 (prot. 2017P9AT72).

Figure captions

Figure 1. Cenozoic magmatic and tectonic activity in East Africa and parts of the Arabian Peninsula (modified from Chorowicz, 2005; Rooney, 2017), superimposed on a NASA-SRTM digital elevation model. The coloured circles indicate the location of samples used in this work; the different colours indicate the three main temporal periods in which the samples are grouped. Enclosed by black dashed lines are the five main tectonic domains in which the samples have been spatially subdivided. Inset shows the location of the East African Rift System.

Figure 2. Correlation plot of CaO/Al_2O_3 vs MgO wt% for the EARS mafic (>4 wt% MgO) magmas during the two oldest periods (a) compared to the youngest period (b) of activity. Symbols and colours identify the different tectonic domains as described in the legend and detailed in the text. The compositional field of MORB and OIB lavas are also shown for comparison.

Figure 3. Distribution of the key trace elements ratio Th/Yb vs Ta/Yb during the oldest two periods of activity (a) and during the youngest period (b) of activity. Symbols and colours identify the different tectonic domains as described in legend and detailed in the text. The compositional field of MORB and OIB lavas are also shown for comparison. Logarithmic scale is used to better highlight sample variation.

Figure 4. Correlation plot of Yb (ppm) vs La/Yb for the products erupted during the two oldest periods (a) and during the youngest period (b-c) of activity showing the effect of mantle melting in the garnet and spinel stability fields, using a non-modal batch melting model. Mantle source compositions are a nominal Primitive Mantle (McDonough and Sun, 1995) (a-b), and a nominal SubContinental Lithospheric Mantle (SCLM, McDonough and Sun 1995) (c). Partition coefficients are from the compilation of McKenzie and O'Nions (1991) and Kelemen et al., 2003. Symbols and colours are reported in the legend. The solid black and red lines represent melts derived from different melting degrees (from 0.1% to 20%) of a garnet and spinel lherzolite, respectively, whereas dashed grey lines represent mixing between garnet- and spinel-derived melts.

Figure 5. Distribution of Rb/Sr vs Ba/Rb trace element ratios showing the role of amphibole-bearing vs phlogopite bearing metasomatized mantle in the genesis of EARS mafic magmas during the oldest two periods (a) and the youngest period of activity (b). The composition of PM and SCLM is also shown (McDonough and Sun, 1995).

Figure 6. Zr/Nb vs Nb/Ta during the two oldest periods (a) and during the youngest period (b) of activity. The compositional field of MORB and OIB lavas are also shown for comparison. Logarithmic scale is used to better highlight sample variation.

Figure 7. Sr-Nd isotope variation through the EARS for the products of the two oldest periods (a) of activity compared to the youngest period of activity (b). The compositional field of MORB and OIB lavas are also shown for comparison. The star represents the composition of the Afar mantle plume proposed by Rooney (2020d) consistent with the values of Afar basalts with high $^{3}He/^{4}He$ of Castillo et al. (2020).

Figure 8. $^{207}Pb/^{204}Pb$ vs $^{206}Pb/^{204}Pb$ through the EARS for the products of the two oldest periods (a) of activity compared to the youngest period of activity (b). The compositional field of MORB and OIB lavas are also shown for comparison. Star as in Figure 7.

Figure 9. Sm-Nd isotope composition of the ultramafic xenoliths. The reference isochrons intercept the y-axis at Nd isotope composition consistent with the evolution of either the primitive (dashed lines) or the depleted mantle (solid lines) at 600 Ma (violet lines) and 2.6 Ga (green lines).

Figure 10. Rhenium-depletion model ages (T_{RD}) from mantle xenoliths of the EARS. The density probability plot is made assuming an uncertainty (1 σ) of 200 Ma on T_{RD} model ages (cf. Pearson et al., 2007) and using the PM composition of $^{187}Os/^{188}Os$=0.1296 and $^{187}Re/^{188}Os$=0.4353 (Meisel et al., 2001). All available literature whole rock data are plotted (Burton et., al 2000, Chesley et al., 1999, Alemayehu et al., 2019, Reisberg et al., 2004, Meisel et al., 2001, Becker et al., 2006). A frequency histogram of T_{RD} ages from different regions is reported in the background. The frequency of each bin is shown on the right axis.

Figure 11. Sr-Nd (a) and Pb (b) isotope signature of ultramafic xenoliths. The isotope compositional field of the mafic magmas characterising the five EARS tectonic districts have been reported for comparison together with the indicative composition of the DMM and Afar Plume (Castillo et al., 2020) mantle components.

Figure 12. Schematic sketch-map cartoon summarising the scenario of magma production along the EARS inferred from the geochemical and isotopic characteristics of mafic magmas correlated with

carbonatites and ultramafic xenoliths and subdivided according to the main tectonic domains (Afar, Ethiopia, Turkana, Eastern Branch, and Western Branch), and to the three main temporal intervals (45-25 Ma, 25-10 Ma and 10-0 Ma), see text for detail. DMM: depleted asthenospheric mantle; SCLM: SubContinental Lithospheric Mantle.

References

Alemayehu M., Guo F. & Aulbach S. (2019) - Transformation of continental lithospheric mantle beneath the East African Rift: constraints from platinum-group elements and Re–Os isotopes in mantle xenoliths from Ethiopia. Contributions to Mineralogy and Petrology, 174, 40 https://doi.org/10.1007/s00410-019-1577-3

Altherr R., Henjes-Kunst F., & Baumann A. (1990) - Asthenosphere versus lithosphere as possible sources for basaltic magmas erupted during formation of the Red Sea: constraints from Sr, Pb and Nd isotopes. Earth and Planetary Science Letters, 96(3-4), 269-286.

Arndt N. T., & Christensen U. (1992) - The role of lithospheric mantle in continental flood volcanism: thermal and geochemical constraints. Journal of Geophysical Research: Solid Earth, 97(B7), 10967-10981.

Ayalewa D., Jungb S., Romerc R.L. & Garbe-Schönbergd D. (2018) - Trace element systematics and Nd, Sr and Pb isotopes of Pliocene flood basalt magmas (Ethiopian rift): A case for Afar plume-lithosphere interaction. Chemical Geology, 493, 172–188. https://doi.org/10.1016/j.chemgeo.2018.05.037

Aulbach S., Creaser R. A., Pearson N. J., Simonetti S. S., Heaman L. M., Griffin W. L. & Stachel T. (2009) - Sulfide and whole rock Re-Os systematics of eclogite and pyroxenite xenoliths from the Slave Craton, Canada. Earth and Planetary Science Letters, 283, 48–58.

Barrat J. A., Joron J. L., Taylor R. N., Fourcade S., Nesbitt R. W. & Jahn B. M. (2003) - Geochemistry of basalts from Manda Hararo, Ethiopia: LREE-depleted basalts in Central Afar. Lithos, 69, 1–13.

Bastow, I.D., Keir, D. (2011) - The protracted development of the continental–ocean transition in Afar. Nature Geoscience 4, 248–250 http://dx.doi.org/10.1038/NGEO1095

Beccaluva L., Bianchini G., Natali C. & Siena F. (2009) - Continental Flood Basalts and Mantle Plumes: a Case Study of the Northern Ethiopian Plateau. Journal of Petrology, 50, 1377–1403.

Becker H., Horan M.F., Walker R.J., Gao S., Lorand J.P. & Rudnick R.L. (2006) - Highly siderophile element composition of the Earth's primitive upper mantle: constraints from new data on peridotite massifs and xenoliths. Geochimica et Cosmochimica Acta, 70, 4528–4550.

Bell K., & Blenkinsop J. (1987) - Nd and Sr isotopic compositions of East African carbonatites: implications for mantle heterogeneity. Geology, 15(2), 99-102.

Biggs J., Ayele A., Fischer T., Fontijn K., Hutchison W., Kazimoto E., Whaler K. & Wright T.J. (2021) - Volcanic activity and hazard in the East African Rift Zone. Nature Communications, 12, 6881. https://doi.org/10.1038/s41467-021-27166-y.

Bizimis M., Salters V. J. M. & Dawson J. B. (2003) - The brevity of carbonatite sources in the mantle: evidence from Hf isotopes. Contributions to Mineralogy and Petrology, 145, 281–300.

Boyce A., Bastow I. D., Cottaar S., Kounoudis R., Guilloud De Courbeville J., Caunt E. & Desai S. (2021) - AFRP20: New *P*-wavespeed model for the African mantle reveals two whole-mantle plumes below East Africa and Neoproterozoic modification of the Tanzania craton. Geochemistry, Geophysics, Geosystems, 22, e2020GC009302. https://doi. org/10.1029/2020GC009302.

Bragagni A., Luguet A., Fonseca R. O. C., Pearson D. G., Lorand J.-P., Nowell G. M. & Kjarsgaard B. A. (2017) - The geological record of base metal sulfides in the cratonic mantle: A microscale 187Os/188Os study of peridotite xenoliths from Somerset Island, Rae Craton (Canada). Geochimica et Cosmochimica Acta, 216, 264–285.

Bragagni A., Mastroianni F., Münker C., Conticelli S. & Avanzinelli R. (2022) - A carbon-rich lithospheric mantle as a source for the large CO_2 emissions of Etna volcano (Italy). Geology, 50, 486–490.

Brooker R. A. & Kjarsgaard B. A. (2011) - Silicate–carbonate liquid immiscibility and phase relations in the system SiO_2–Na_2O–Al_2O_3–CaO–CO_2 at 0·1–2·5 GPa with applications to carbonatite genesis. Journal of Petrology, 52(7-8), 1281-1305.

Burton K.W., Schiano P., Birck J.-L., Allègre C.J., Rehkämper M., Halliday A.N. & Dawson J.B. (2000) - The distribution and behaviour of rhenium and osmium amongst mantle minerals and the age of the lithospheric mantle beneath Tanzania. Earth and Planetary Science Letters, 183, 93–106.

Castillo P. R., Hilton D. R. & Halldórsson S. A. (2014) - Trace element and Sr-Nd-Pb isotope geochemistry of Rungwe Volcanic Province, Tanzania: implications for a Superplume source for East Africa Rift magmatism. Frontiers in Earth Science, 2, 21.

Castillo P. R., Liu X. & Scarsi P. (2020) - The geochemistry and Sr-Nd-Pb isotopic ratios of high 3He/4He Afar and MER basalts indicate a significant role of the African Superplume in EARS magmatism. Lithos, 376–377, 105791.

Chakhmouradian A. R. (2006) - High-field-strength elements in carbonatitic rocks: Geochemistry, crystal chemistry and significance for constraining the sources of carbonatites. Chemical Geology, 235, 138–160.

Chesley J.T., Rudnick R.L. & Lee C.T. (1999) - Re–Os systematics of mantle xenoliths from the East African Rift: age, structure, and history of the Tanzanian craton. Geochimica et Cosmochimica Acta, 63, 1203–1217.

Chorowicz J. (2005) - The East African Rift System. Journal of African Earth Sciences, 43, 379–410, doi: 10.1016/j.jafrearsci.2005.07.019.

Civiero, C., Lebedev, S., & Celli, N. L. (2022) - A complex mantle plume head below East Africa-Arabia shaped by the lithosphere-asthenosphere boundary topography. Geochemistry, Geophysics, Geosystems, 23, e2022GC010610. https://doi.org/10.1029/2022GC010610

Coblentz D.D., Sandiford M. (1994). Tectonic stresses in the African plate: constraints on the ambient lithospheric stress state. Geology, 22, 831–834.

Conticelli S., Sintoni M. F., Abebe T., Mazzarini F. & Manetti P. (1999) - Petrology and geochemistry of ultramafic xenoliths and host lavas from the Ethiopian Volcanic Province: An insight into the upper mantle under eastern Africa. Acta Vulcanologica, 11, 143-160.

Corti, G. (2009) - Continental rift evolution: from rift initiation to incipient break-up in the Main Ethiopian Rift, East Africa. Earth-Science Reviews, 96(1-2), 1-53.

Corti G., Maestrelli D. & Sani F. (2022) - Large-to local-scale control of pre-existing structures on continental rifting: examples from the Main Ethiopian Rift, East Africa. Frontiers in Earth Science, 10:808503, doi: 10.3389/feart.2022.808503.

Daoud M. A., Maury R. C., Barrat J.-A., Taylor R. N., Le Gall B., Guillou H., Cotten J. & Rolet J. (2010) - A LREE-depleted component in the Afar plume: Further evidence from Quaternary Djibouti basalts. Lithos, 114, 327–336.

Ebinger C.J. (2020) - Recipe for Rifting: Flavors of East Africa. Encyclopedia of Geology, 2nd edition, Elsevier, 1-13. https://doi.org/10.1016/B978-0-08-102908-4.00100-4

Ebinger C.J., Poudjom Djomani, Y., Mbede, E., Foster A. and Dawson J.B. (1997) - Rifting Archaean lithosphere: the Eyasi–Manyara–Natron rifts, East Africa. Journal of the Geological Society, London, 154, 947–960.

Eggler D. H., & Bell, K. (1989) - Carbonatites, primary melts, and mantle dynamics. Carbonatites: genesis and evolution, 561-579.

Feyissa D. H., Shinjo R., Kitagawa H., Meshesha D. & Nakamura E. (2017) - Petrologic and geochemical characterization of rift-related magmatism at the northernmost Main Ethiopian Rift: Implications for plume-lithosphere interaction and the evolution of rift mantle sources. Lithos, 282–283, 240–261.

Feyissa D. H., Kitagawa H., Bizuneh T. D., Tanaka R., Kabeto K. & Nakamura E. (2019) - Transition from Plume-driven to Plate-driven Magmatism in the Evolution of the Main Ethiopian Rift. Journal of Petrology, 60, 1681–1715.

Fishwick S. (2010) - Surface wave tomography: imaging of the lithosphere asthenosphere boundary beneath central and southern Africa. Lithos, 120, 63–73.

Fishwick S. & Bastow I.D. (2011) - Towards a better understanding of African topography: a review of passive-source seismic studies of the African crust and upper mantle. In: Van Hinsbergen, D. J. J., Buiter, S. J. H., Torsvik, T. H., Gaina, C. &Webb, S. J. (eds) The Formation and Evolution of Africa: A Synopsis of 3.8 Ga of Earth History. Geological Society, London, Special Publications, 357, 343–371. DOI: 10.1144/SP357.19.

Foley S. F., Link K., Tiberindwa J. V. & Barifaijo E. (2012) - Patterns and origin of igneous activity around the Tanzanian craton. Journal of African Earth Sciecens, 62, 1–18.

Franceschini Z., Cioni R., Scaillet S., Corti G., Sani F., Isola I., Mazzarini F., Duval F., Erbello A., Muluneh A. & Brune S. (2020) - Recent volcano-tectonic activity of the Ririba rift and the evolution of rifting in South Ethiopia. Journal of Volcanology and Geothermal Research, 402, 106989.

Furman T. & Graham D. (1999) - Erosion of lithospheric mantle beneath the East African Rift system: geochemical evidence from the Kivu volcanic province. Lithos, 48, 237–262.

Furman T., Kaleta K., Bryce J. & Hanan B.B. (2006) - Tertiary mafic lavas of Turkana, Kenya: constraints on East African plume structure and the occurrence of high-micro volcanism in Africa. Journal of Petrology, 47, 1221–1244.

Furman T. (2007) - Geochemistry of East African Rift basalts: An overview. Journal of African Earth Sciences, 48, 147–160.

Furman, T., Nelson, W. R., & Elkins-Tanton, L. T. (2016)- Evolution of the East African rift: drip magmatism, lithospheric thinning and mafic volcanism. Geochimica et Cosmochimica Acta, 185, 418-434.

Gasparon M., Innocenti F., Manetti P., Peccerillo A., & Tsegaye A. (1993) - Genesis of the Pliocene to Recent bimodal mafic-felsic volcanism in the Debre Zeyt area, central Ethiopia: Volcanological and geochemical constraints. Journal of African Earth Sciences (and the Middle East), 17(2), 145-165.

George R., Rogers N. & Kelley S. (1998) - Earliest magmatism in Ethiopia: evidence for two mantle plumes in one flood basalt province. Geology, 26, 923-926.

George R., & Rogers N. (2002) - Plume dynamics beneath the African plate inferred from the geochemistry of the Tertiary basalts of southern Ethiopia. Contributions to Mineralogy and Petrology, 144(3), 286-304.

Graham, D.W., Jenkins, W. J., Schilling, J.G., Thompson, G., Kurz, M. D., & Humphris, S.E. (1992) - Helium isotope geochemistry of mid-ocean ridge basalts from the South Atlantic. Earth and Planetary Science Letters, 110(1-4), 133-147.

Graham, D.W., Larsen, L.M., Hanan, B.B., Storey, M., Pedersen, A.K., & Lupton, J. E. (1998) - Helium isotope composition of the early Iceland mantle plume inferred from the Tertiary picrites of West Greenland. Earth and Planetary Science Letters, 160(3-4), 241-255.

Green T. H. (1995) - Significance of Nb/Ta as an indicator of geochemical processes in the crust-mantle system. Chemical Geology, 120, 347–359.

Guzmics T., Berkesi M., Bodnar R. J., Fall A., Bali E., Milke R. & Szabó C. (2019) - Natrocarbonatites: A hidden product of three-phase immiscibility. Geology, 47(6), 527-530.

Halldórsson S. A., Hilton D. R., Scarsi P., Abebe T. & Hopp J. (2014) - A common mantle plume source beneath the entire East African Rift System revealed by coupled helium-neon systematics. Geophysical Research Letters, 41, 2304–2311.

Halldórsson S. A., Hilton D. R., Marshall E. W., Ranta E., Ingvason A., Chakraborty S., Robin J. G., Rasmussen M. B., Gibson S. A., Ono S., Scarsi P., Abebe T., Hopp J., Barry P. H. & Castillo P. R. (2022) - Evidence from gas-rich ultramafic xenoliths for Superplume-derived recycled volatiles in the East African sub-continental mantle. Chemical Geology, 589, 120682.

Hanan B.B., & Graham D.W. (1996) - Lead and helium isotope evidence from oceanic basalts for a common deep source of mantle plumes. Science, 272(5264), 991-995.

Hassan R., Williams S.E., Gurnis M. & Müller D. (2020) - East African topography and volcanism explained by a single, migrating plume. Geoscience Frontiers, 11(5), 1669-1680.

Hawkesworth C. J., Rogers N. W., Van Calsteren P. W. C. & Menzies M. A. (1984) - Mantle enrichment processes. Nature, 311(5984), 331-335.

Hoernle K., Tilton G., Le Bas M. J., Duggen S. & Garbe-Schönberg D. (2002) - Geochemistry of oceanic carbonatites compared with continental carbonatites: mantle recycling of oceanic crustal carbonate. Contributions to Mineralogy and Petrology, 142, 520–542.

Hoffman C., Courtillot V., Féraud G., Rochette P., Yirgu G., Ketefo E., Pik R. (1997) - Timing of the Ethiopian basalt event and implications for plume birth and global change. Nature, 389, 838-841.

Hopper E., Gaherty J.B., Shillington D.J., Accardo N.J., Nyblade A.A., Holtzman B.K., Havlin C., Scholz C.A., Patrick R. N. Chindandali R.N., Ferdinand R.W., Mulibo G.D. & Mbogoni G. (2020) - Preferential localized thinning of lithospheric mantle in the melt-poor Malawi Rift. Nature Geoscience, 13, 584–589. https://doi.org/10.1038/s41561-020-0609-y.

Kendall J.M., Stuart G.W., Ebinger C.J., Bastow I.D. & Keir D. (2005) - Magma assisted rifting in Ethiopia. Nature, 433, 146–148.

Kelemen P. B., Hanghøj K., & Greene A. R. (2003) - One view of the geochemistry of subduction-related magmatic arcs, with an emphasis on primitive andesite and lower crust. Treatise on Geochemistry, 3, 659.

Keranen, K., Klemperer, S.L., Gloaguen, R., EAGLE Working Group (2004) - Three-dimensional seismic imaging of a protoridge axis in the Main Ethiopian rift. Geology 32, 949–952 http://dx.doi.org/10.1130/G20737.1.

Kieffer B., Arndt N., LaPierre H., Bastien F., Bosch D., Pecher A., Yirgu G., Ayalew D., Weis D., Jerram D., Keller F. & Meugniot C. (2004) - Flood and Shield Basalts from Ethiopia: Magmas from the African Superswell. Journal of Petrology, 45, 793-834.

Koptev A. Calais E., Burov E., Leroy S. & Gerya T. (2015) - Dual continental rift systems generated by plume–lithosphere interaction. Nature Geoscience, 8, 388-392. DOI: 10.1038/NGEO2401.

Ionov D. A., Bodinier J.-L., Mukasa S. B. & Zanetti A. (2002) - Mechanisms and Sources of Mantle Metasomatism: Major and Trace Element Compositions of Peridotite Xenoliths from Spitsbergen in the Context of Numerical Modelling. Journal of Petrology, 43, 2219–2259.

Lawrence L., Spandler C., Hilbert-Wolf H. L., Mtelela C., Stevens N. J., O'Connor P. M. & Roberts E. M. (2022) - Radiogenic isotope record of magma genesis and lithospheric geodynamics of the Rukwa Rift Basin, Tanzania, from mid Mesozoic to present. Chemical Geology, 608, 121040.

Lloyd F. E., Woolley A. R., Stoppa F., & Eby G. N. (2002) - Phlogopite-biotite parageneses from the K-mafic-carbonatite effusive magmatic association of Katwe-Kikorongo, SW Uganda. Mineralogy and Petrology, 74(2), 299-322.

McDonough W.S. (1990) - Constraints on the composition of the continental lithospheric mantle. Earth and Planetary Science Letters, 101(1), 1-18.

McDonough W.F. & Sun S.S. (1995) - The composition of the Earth. Chemical Geology, 120(3-4), 223-253.

Mckenzie D. A. N. & Bickle M. J. (1988) - The volume and composition of melt generated by extension of the lithosphere. Journal of Petrology, 29(3), 625-679.

McKenzie D. A. N. & O'Nions R. K. (1991) - Partial melt distributions from inversion of rare earth element concentrations. Journal of Petrology, 32(5), 1021-1091.

Meisel T., Walker R.J., Irving A.J., Lorand J.-P. (2001) - Osmium isotopic compositions of mantle xenoliths: a global perspective. Geochimica et Cosmochimica Acta, 65, 1311–1323.

Menzies M., & Hawkesworth C. (1987) - Mantle metasomatism. London and New York Academic Press, 472 pp.

Meshesha D., Shinjo R., Matsumura R. and Chekol T. (2011) - Metasomatized lithospheric mantle beneath Turkana depression in southern Ethiopia (the East Africa Rift): geochemical and Sr–Nd–Pb isotopic characteristics. Contributions to Mineralogy and Petrology, 162, 889–907.

Morley C. & Chantraprasert S. (2022) - Plume-related, syn-rift, Neogene volcanism, the interplay with structure in Thailand and comparison with the East African Rift. Ital. J. Geosci., 141(3), 295-333, https://doi.org/10.3301/IJG.2022.24.2022

Moucha R. & Forte A.M. (2011) - Changes in African topography driven by mantle convection. Nature Geoscience, 4(10):707-712, DOI: 10.1038/ngeo1235

Muirhead J. D., Scholz C.A., Rooney T.O. (2022) - Transition to magma-driven rifting in the South Turkana Basin, Kenya: Part 1. Journal of the Geological Society of London, 179, jgs2021-159, https://doi.org/10.1144/jgs2021-159

Muirhead J. D., Fischer T. P., Oliva S. J., Laizer A., Wijk J. van, Currie C. A., Lee H., Judd E. J., Kazimoto E., Sano Y., Takahata N., Tiberi C., Foley S. F., Dufek J., Reiss M. C. & Ebinger C. J.

(2020) - Displaced cratonic mantle concentrates deep carbon during continental rifting. Nature, 582, 67–72.

Muravyeva N. S. & Senin V. G. (2018) - Xenoliths from Bunyaruguru volcanic field: Some insights into lithology of East African Rift upper mantle. Lithos, 296–299, 17–36.

Natali C., Beccaluva L., Bianchini G., Ellam R. M., Savo A., Siena F. & Stuart F. M. (2016) - High-MgO lavas associated to CFB as indicators of plume-related thermochemical effects: The case of ultra-titaniferous picrite–basalt from the Northern Ethiopian–Yemeni Plateau. Gondwana Research, 34, 29–48.

Nelson W. R., Furman T., van Keken P. E., Shirey S. B. & Hanan B. B. (2012) – Os Hf isotopic insight into mantle plume dynamics beneath the East African Rift System. Chemical Geology, 320–321, 66–79.

Nelson W. R., Hanan B. B., Graham D. W., Shirey S. B., Yirgu G., Ayalew D. & Furman T. (2019) - Distinguishing Plume and Metasomatized Lithospheric Mantle Contributions to Post-Flood Basalt Volcanism on the Southeastern Ethiopian Plateau. Journal of Petrology, 60, 1063–1094.

Njinju E.A., Atekwana E.A., Stamps D.S., Abdelsalam M.G., Atekwana E.A., Mickus K.S., Fishwick S., Kolawole F., Rajaonarison T.A. & Nyalugwe V.N. (2019) - Lithospheric structure of the Malawi Rift: implications for magma-poor rifting processes. Tectonics, 38, 3835–3853.

Pearson D. G., Parman S. W. & Nowell G. M. (2007) - A link between large mantle melting events and continent growth seen in osmium isotopes. Nature, 449, 202–205.

Pfänder J. A., Jung S., Münker C., Stracke A. & Mezger K. (2012) - A possible high Nb/Ta reservoir in the continental lithospheric mantle and consequences on the global Nb budget – Evidence from continental basalts from Central Germany. Geochimica et Cosmochimica Acta, 77, 232–251.

Pik R., Deniel C., Coulon C., Yirgu G. & Marty B. (1999) - Isotopic and trace element signatures of Ethiopian flood basalts: evidence for plume–lithosphere interactions. Geochimica et Cosmochimica Acta, 63, 2263–2279.

Purcell P.G. (2017) - Re-imagining and re-imaging the development of the East African Rift. Petroleum Geoscience, 24, 21-40. https://doi.org/10.1144/petgeo2017-036.

Reisberg L., Lorand J.B. & Bedini R.M. (2004) - Reliability of Os model ages in pervasively metasomatized continental lithosphere: a case study of Sidamo spinel peridotite xenoliths (East African Rift, Ethiopia). Chemical Geology, 208, 119–140.

Rychert C., Hammond J., Harmon N., Kendall J., Keir D., Ebinger C., Bastow I., Ayele A., Belachew M., Stuart G. (2012) - Volcanism in the Afar Rift sustained by decompression melting with minimal plume influence. Nature Geoscience. 5. 406-409. 10.1038/ngeo1455.

Ritsema J., van Heijst H.J. & Woodhouse J.H. (1999) - Complex shear wave velocity structure imaged beneath Africa and Iceland. Science, 286, 1925–1928.

Roberts E.M., Stevens N.J., O'Connor P.M., Dirks P.H.G.M., Gottfried M.D., Clyde W.C., Armstrong R.A., Kemp A.I.S. & Hemming S. (2012) - Initiation of the western branch of the East African Rift coeval with the eastern branch. Nature Geoscience, 5, 289-294. DOI: 10.1038/NGEO1432.

Rogers N.W., James D., Kelley S. P. & De Mulder M. (1998) - The Generation of Potassic Lavas from the Eastern Virunga Province, Rwanda. Journal of Petrology, 39, 1223–1247.

Rogers N., Macdonald R. & Godfrey J. (2000) - Two mantle plumes beneath the East African rift system: Sr, Nd, and Pb isotope evidence from Kenya Rift basalts. Earth and Planetary Science Letters, 176, 387–400.

Rogers N.W. (2006) - Basaltic magmatism and the geodynamics of the East African Rift System. Geological Society, London, Special Publications, 259(1), 77-93.

Rooney T.O., Nelson W.R., Dosso L., Furman T. & Hanan B. (2014) - The role of continental lithosphere metasomes in the production of HIMU-like magmatism on the northeast African and Arabian plates. Geology, 42, 419–422.

Rooney T.O. (2017) - The Cenozoic magmatism of East-Africa: Part I–Flood basalts and pulsed magmatism. Lithos, 286, 264–301. http://dx.doi.org/10.1016/j.lithos.2017.05.014.

1101 Rooney T.O. (2020a) - The Cenozoic magmatism of East Africa: Part II – Rifting of the mobile belt.
1102 Lithos, 360–361, 105291. https://doi.org/10.1016/j.lithos.2019.105291.
1103 Rooney T.O. (2020b) - The Cenozoic magmatism of East Africa: part III–rifting of the
1104 craton. Lithos, 360, 105390.
1105 Rooney T.O. (2020c) - The Cenozoic magmatism of East Africa: part IV–the terminal stages of rifting
1106 preserved in the Northern East African Rift System. Lithos, 360, 105381.
1107 Rooney T.O. (2020d) - The Cenozoic magmatism of East Africa: Part V – Magma sources and processes
1108 in the East African Rift. Lithos, 360–361, 105296. https://doi.org/10.1016/j.lithos.2019.105296.
1109 Rooney T.O., Hanan B.B., Graham D.W., Furman T., Blichert-Toft J. & Schilling J.-G. (2012) - Upper
1110 mantle pollution during Afar Plume–Continental rift interaction. Journal of Petrology, 53, 365–389.
1111 https://doi.org/10.1093/petrology/egr065.
1112 Rosenthal A., Foley S. F., Pearson D. G., Nowell G. M. & Tappe S. (2009) - Petrogenesis of strongly
1113 alkaline primitive volcanic rocks at the propagating tip of the western branch of the East African Rift.
1114 Earth and Planetary Science Letters, 284, 236–248.
1115 Simon B., Guillocheau F., Robin C., Dauteuil O., Nalpas T., Pickford M., Senut B., Lays P., Bourges P.
1116 & Bez M. (2017) - Deformation and sedimentary evolution of the Lake Albert Rift (Uganda, East
1117 African Rift System). Marine and Petroleum Geology, 86, 17-37.
1118 http://dx.doi.org/10.1016/j.marpetgeo.2017.05.006.
1119 Spath A. (2001) - Plume-Lithosphere Interaction and the Origin of Continental Rift-related Alkaline
1120 Volcanism--the Chyulu Hills Volcanic Province, Southern Kenya. Journal of Petrology, 42, 765–787.
1121 Stamps D.S., Flesch L.M., Calais E. & Ghosh A. (2014) - Current kinematics and dynamics of Africa
1122 and the East African Rift System, Journal of Geophysical Research Solid Earth, 119, 5161–5186,
1123 doi:10.1002/2013JB010717.
1124 Steiner R.A., Rooney T.O., Girard G., Rogers N., Ebinger C.J., Peterson L. & Phillips R.K. (2022) -
1125 Initial Cenozoic magmatic activity in East Africa: new geochemical constraints on magma
1126 distribution within the Eocene continental flood basalt province. Geological Society, London, Special
1127 Publications, 518, 435–465.
1128 Stamps, D.S., Iaffaldano G. & Calais E. (2015) - Role of mantle flow in Nubia-Somalia plate divergence,
1129 Geophysical Research Letters, 42, 290–296, doi:10.1002/2014GL062515.
1130 Stolz A. J., & Davies G. R. (1988) - Chemical and isotopic evidence from spinel lherzolite xenoliths for
1131 episodic metasomatism of the upper mantle beneath southeast Australia. Journal of Petrology, (1),
1132 303-330.
1133 Stracke A., Hofmann A. W. & Hart S. R. (2005) - FOZO, HIMU, and the rest of the mantle
1134 zoo. Geochemistry, Geophysics, Geosystems, 6(5).
1135 Sun S. S. & McDonough W. F. (1989) - Chemical and isotopic systematics of oceanic basalts:
1136 implications for mantle composition and processes. Geological Society, London, Special
1137 Publications, 42(1), 313-345.
1138 Tappe S., Budde G., Stracke A., Wilson A. & Kleine T. (2020) - The tungsten-182 record of kimberlites
1139 above the African superplume: Exploring links to the core-mantle boundary. Earth and Planetary
1140 Science Letters, 547, 116473.
1141 Tortelli, G., Gioncada, A., Pagli, C., Braschi, E., Gebru, E. F., & Keir, D. (2022) - Constraints on the
1142 magma source and rift evolution from geochemistry of the Stratoid flood basalts (Afar, Ethiopia).
1143 Geochemistry, Geophysics, Geosystems, 23, e2022GC010434.
1144 https://doi.org/10.1029/2022GC010434
1145 Van Straaten P. and Bell K. (1989) Nature and structural relationships of carbonatites from Southwest
1146 and West Tanzania. Carbonatites: Genesis and Evolution. Unwin Hyman, London, 177–199.
1147 Vollmer R. & Norry M. J. (1983) -Unusual isotopic variations in Nyiragongo nephelinites. Nature 301,
1148 141–143.
1149 Walker R. J., Carlson R. W., Shirey S. B. & Boyd F. R. (1989) - Os, Sr, Nd, and Pb isotope systematics
1150 of southern African peridotite xenoliths: implications for the chemical evolution of subcontinental
1151 mantle. Geochimica et Cosmochimica Acta, 53(7), 1583-1595.

1152 Wong K., Ferguson D., Matthews S., Morgan D., Tadesse A.Z., Sinetebeb Y. & Yirgu G. (2022) - 1153 Exploring rift geodynamics in Ethiopia through olivine-spinel Al-exchange thermometry and rare- 1154 earth element distributions. Earth and Planetary Science Letters, 597, 117820.
1155 Zwaan F., Corti G., Sani F., Keir D., Muluneh A., Illsley-Kemp F. & Papini M. (2020) - Structural 1156 analysis of the Western Afar Margin, East Africa: evidence for multiphase rotational rifting. 1157 Tectonics, 39, e2019TC006043, https://doi.org/10.1029/2019TC006043.

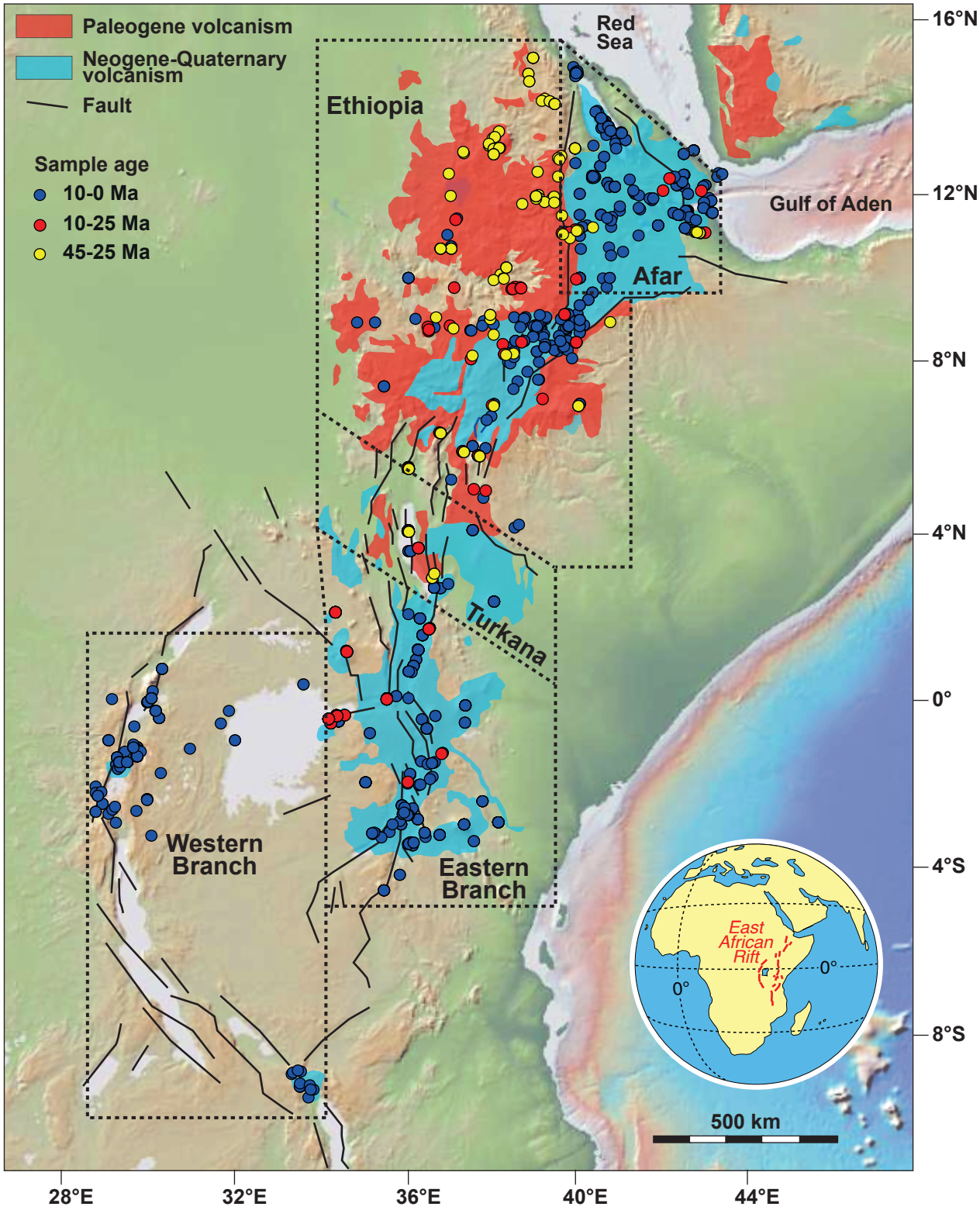
Paleogene volcanism
Neogene-Quaternary volcanism
Fault
Sample age
10-0 Ma
10-25 Ma
45-25 Ma
Red Sea
Ethiopia
Gulf of Aden
Afar
Turkana
Western Branch
Eastern Branch
East African Rift
0°
0°
500 km
16°N
12°N
8°N
4°N
0°
4°S
8°S
28°E
32°E
36°E
40°E
44°E

Figure 1

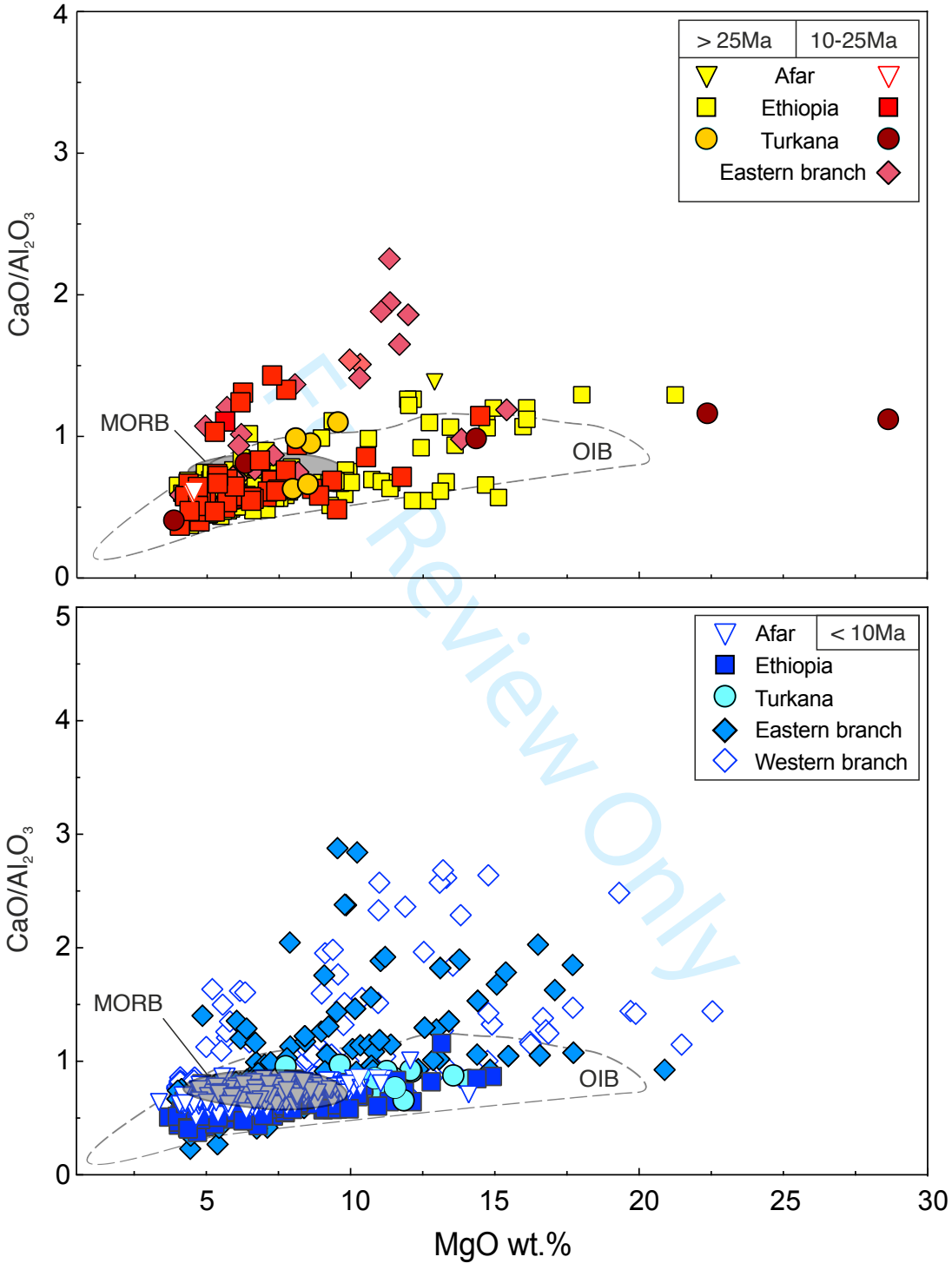

Figure 2

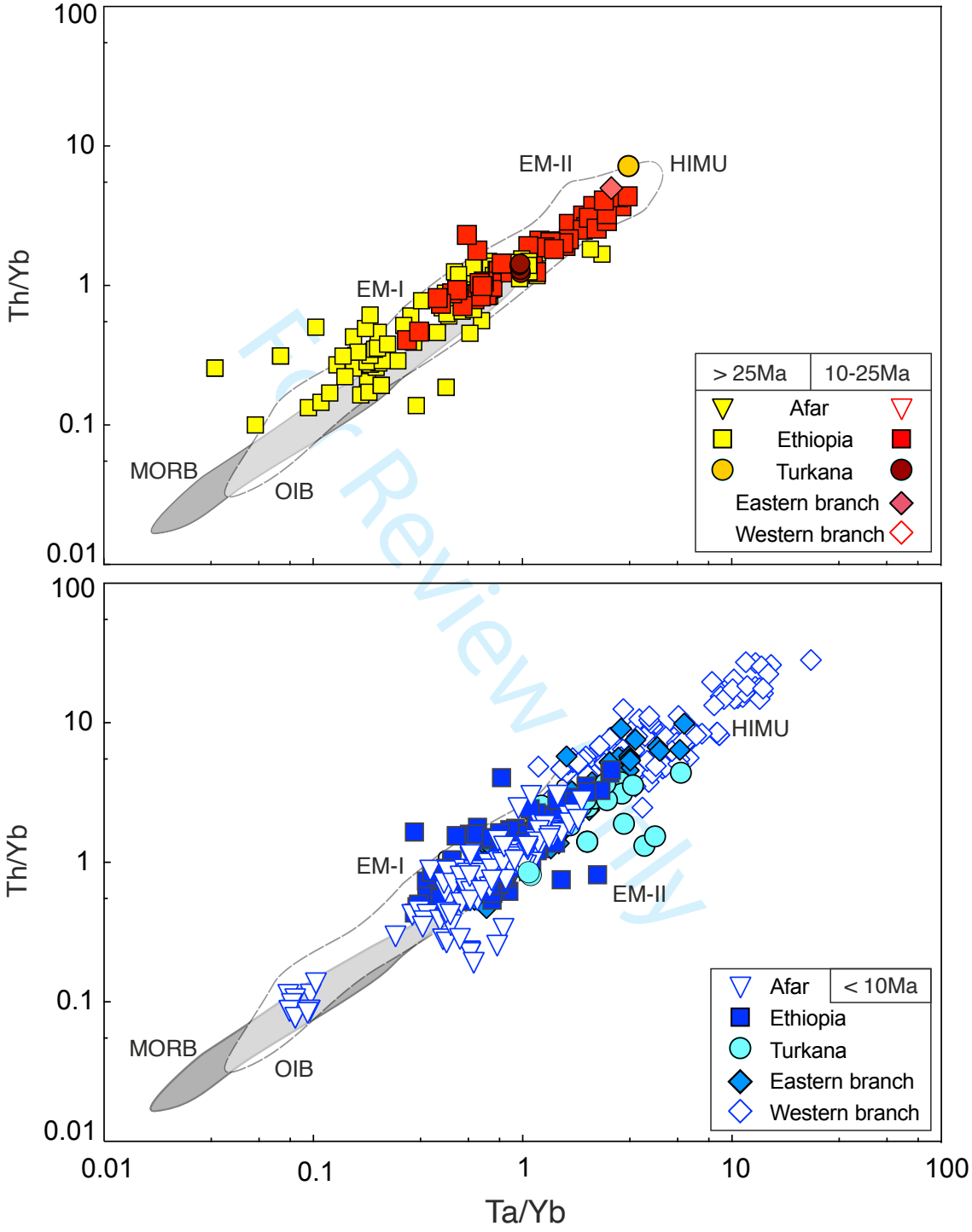
Th/Yb
100
10
1
0.1
0.01
EM-II
HIMU
EM-I
MORB
OIB
> 25Ma
10-25Ma
Afar
Ethiopia
Turkana
Eastern branch
Western branch
Th/Yb
HIMU
EM-I
EM-II
< 10Ma
0.01
0.1
1
10
100
Ta/Yb

Figure 3

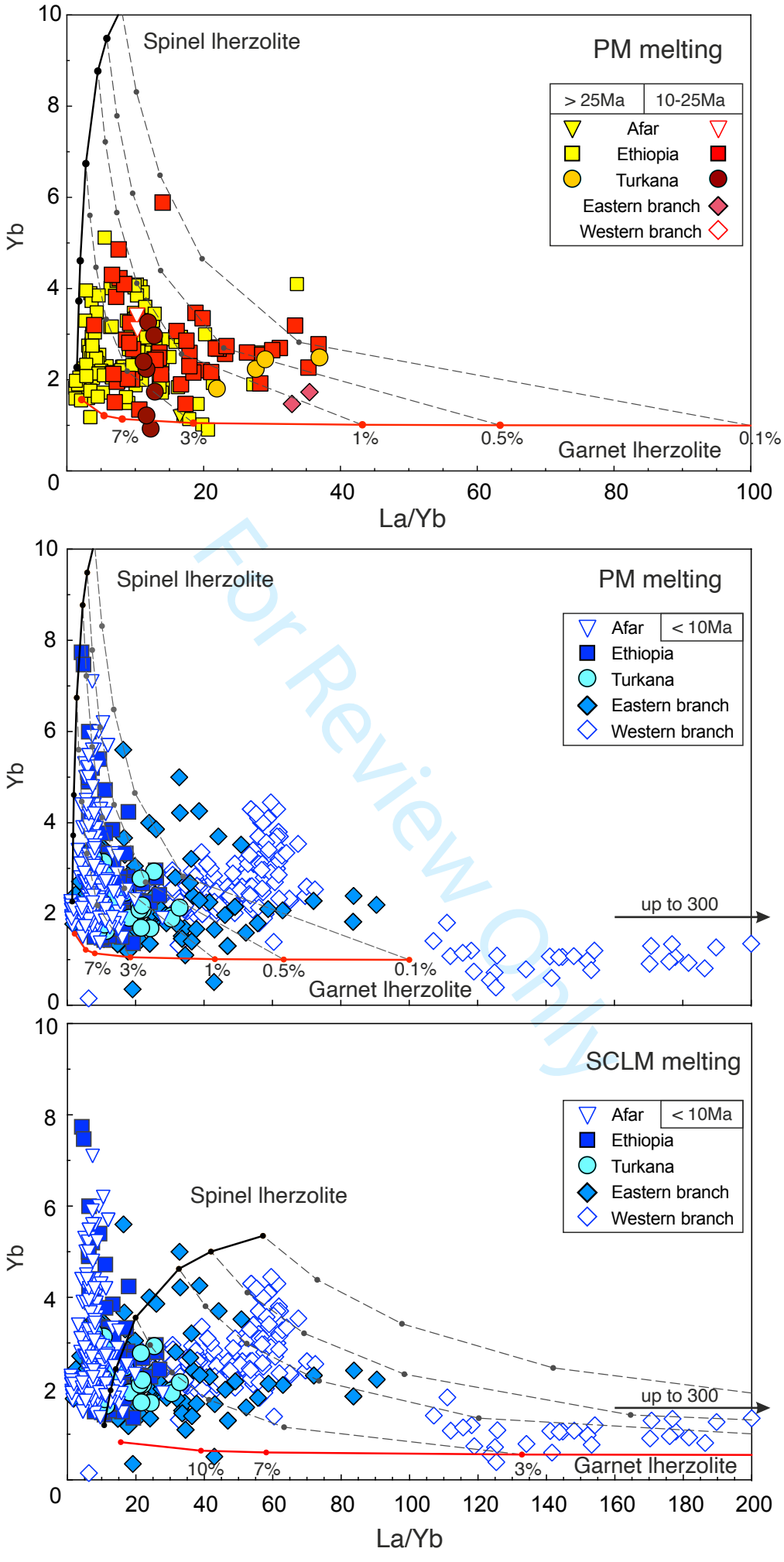

Figure 4

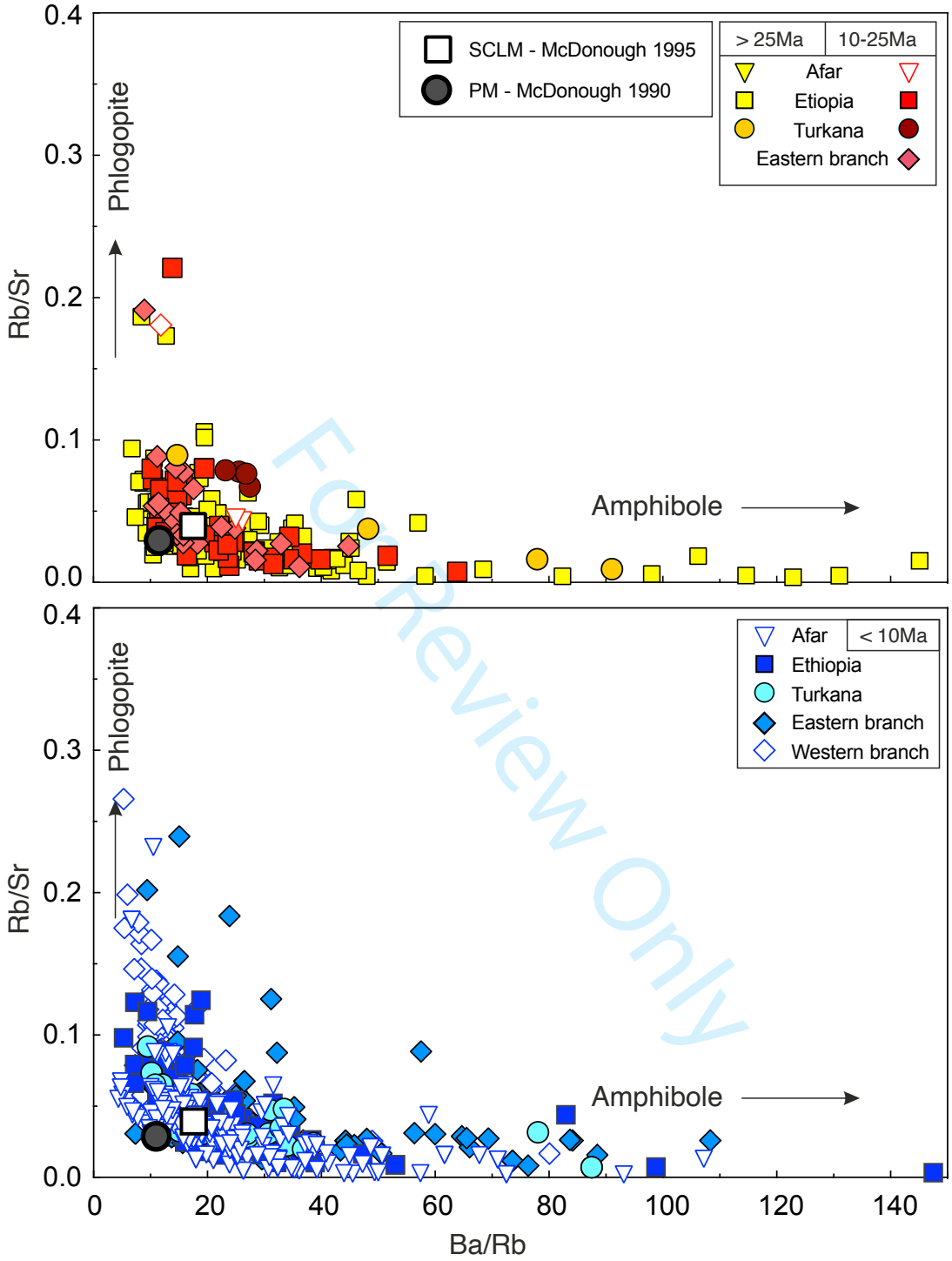

Figure 5

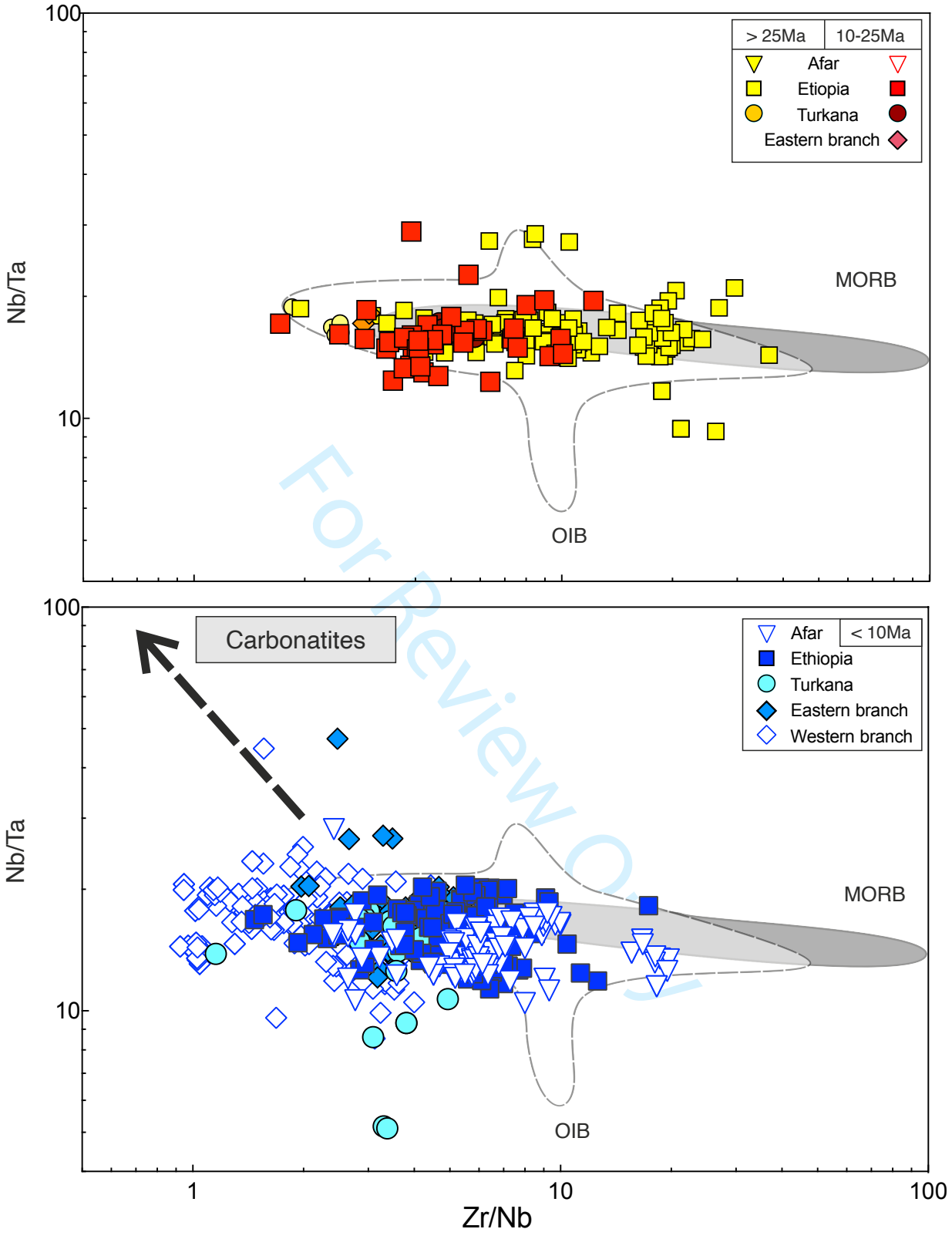

Figure 6

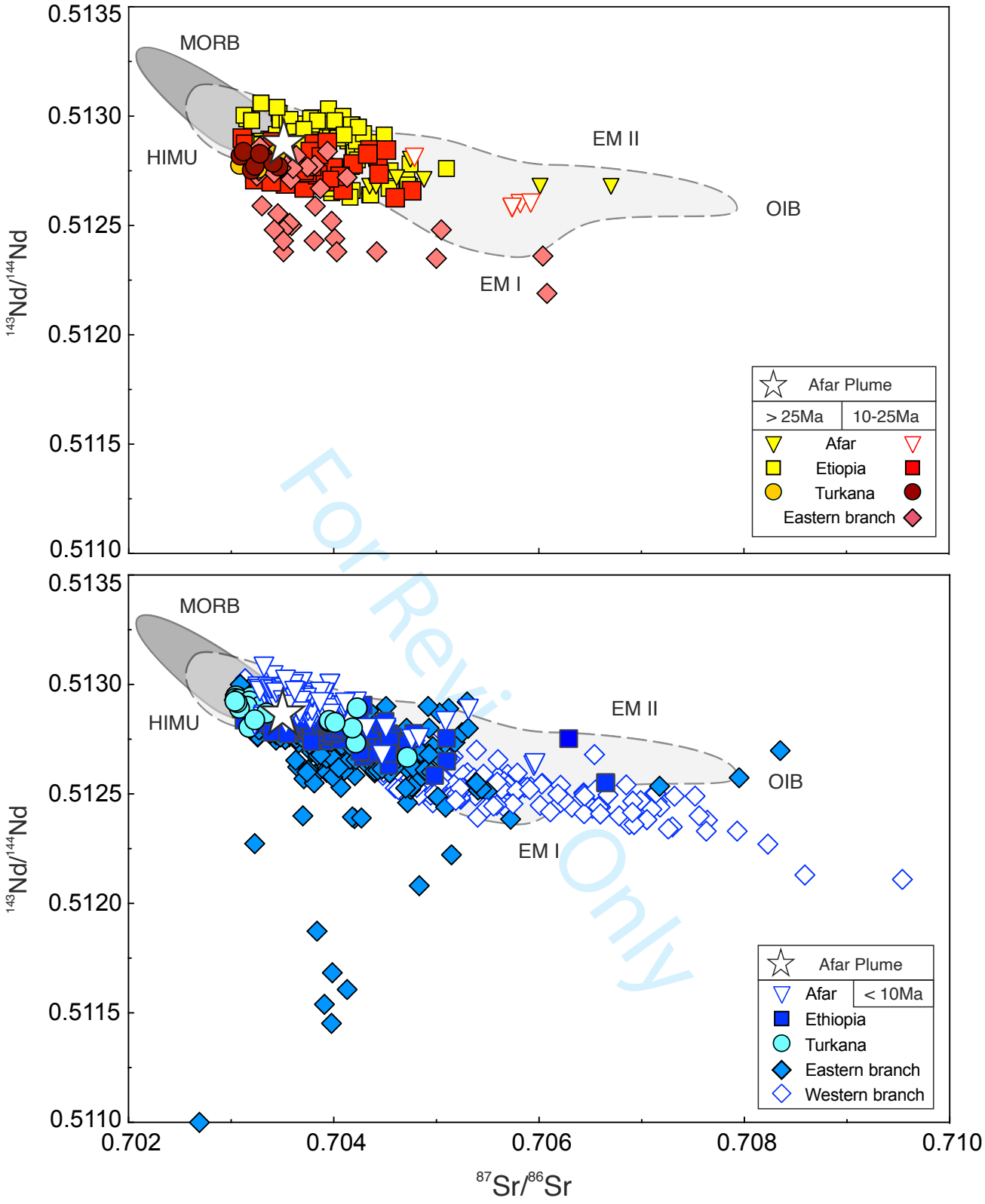
MORB
HIMU
EM II
EM I
OIB
Afar Plume
> 25Ma
10-25Ma
Afar
Etiopia
Turkana
Eastern branch
< 10Ma
Western branch
0.5135
0.5130
0.5125
0.5120
0.5115
0.5110
0.702
0.704
0.706
0.708
0.710
143Nd/144Nd
87Sr/86Sr

Figure 7

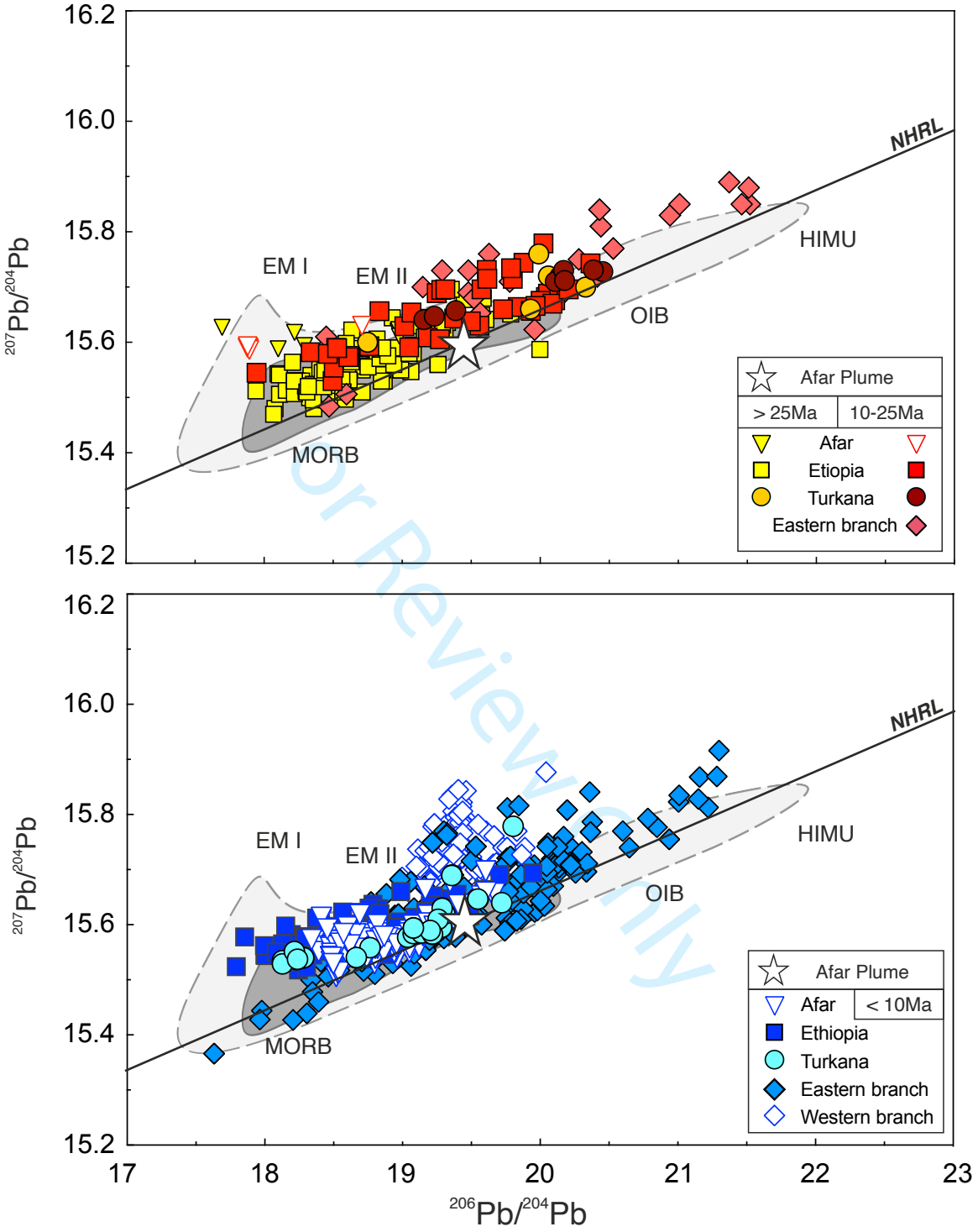

Figure 8

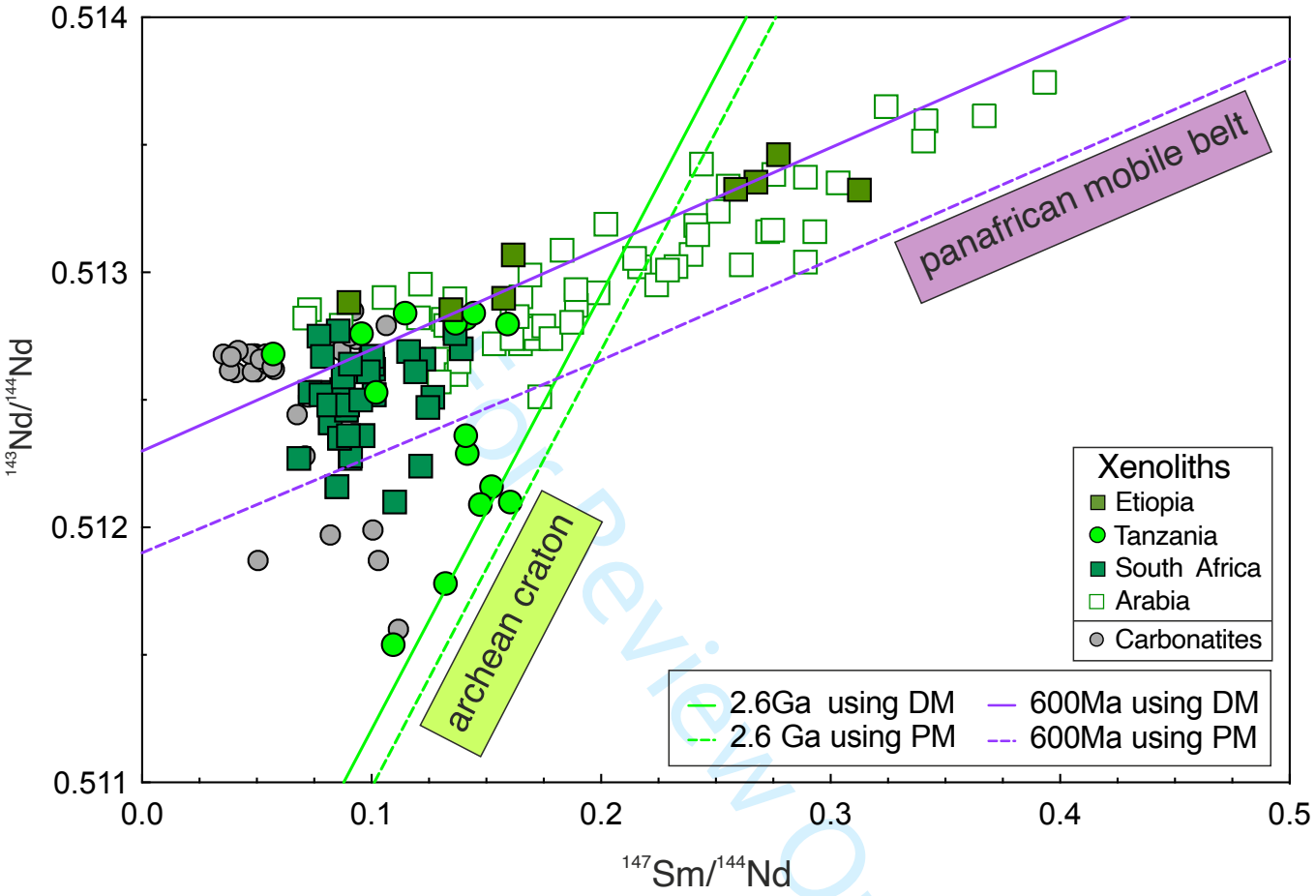

Figure 9

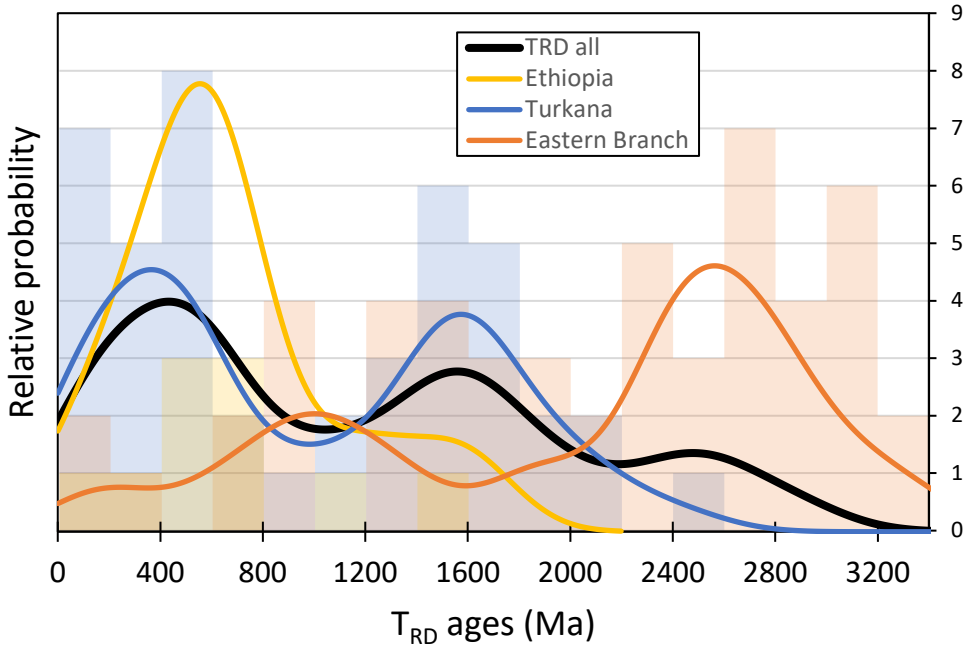
TRD all
Ethiopia
Turkana
Eastern Branch
Relative probability
0
1
2
3
4
5
6
7
8
9
0
400
800
1200
1600
2000
2400
2800
3200
T_RD ages (Ma)

Figure 10

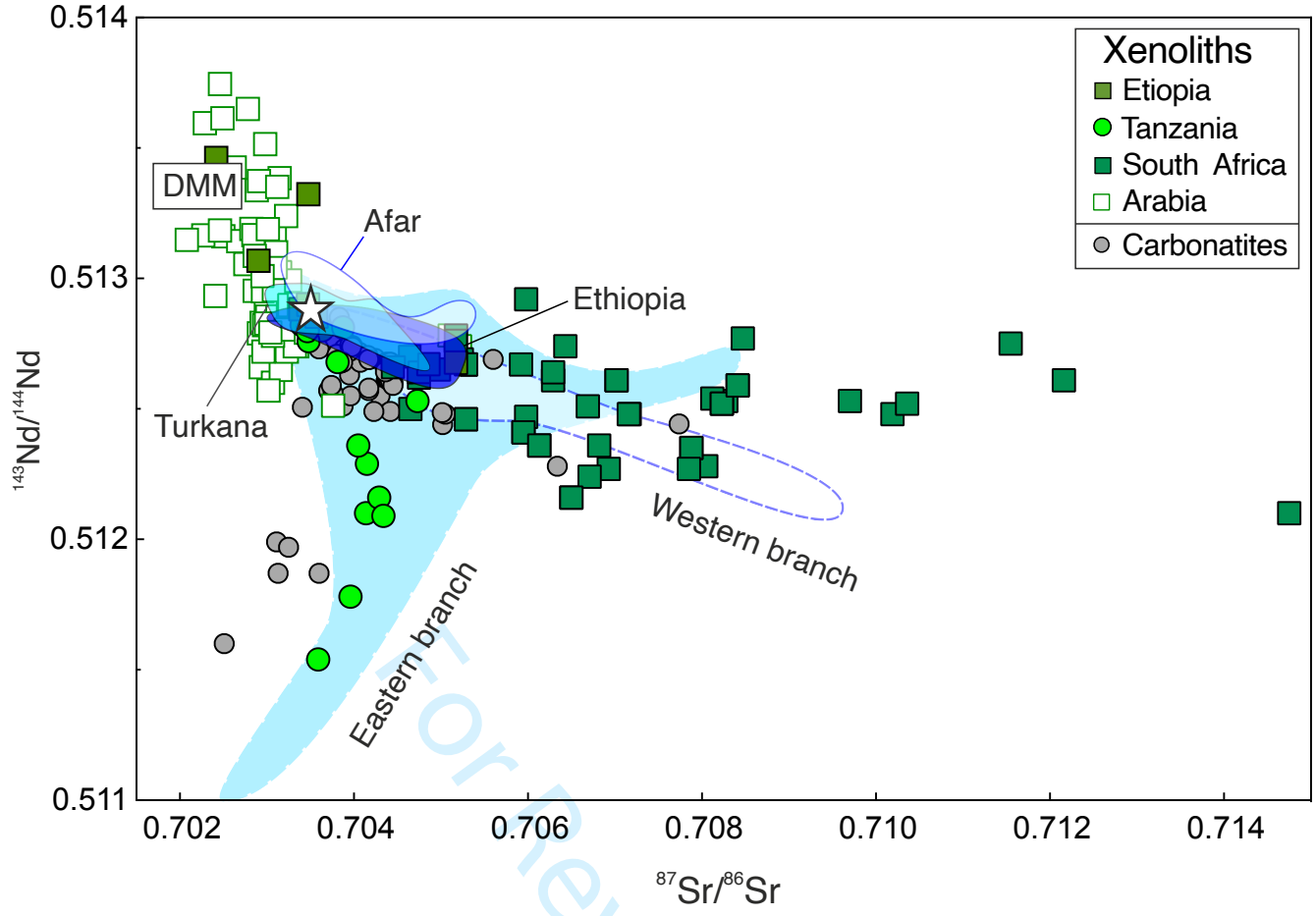

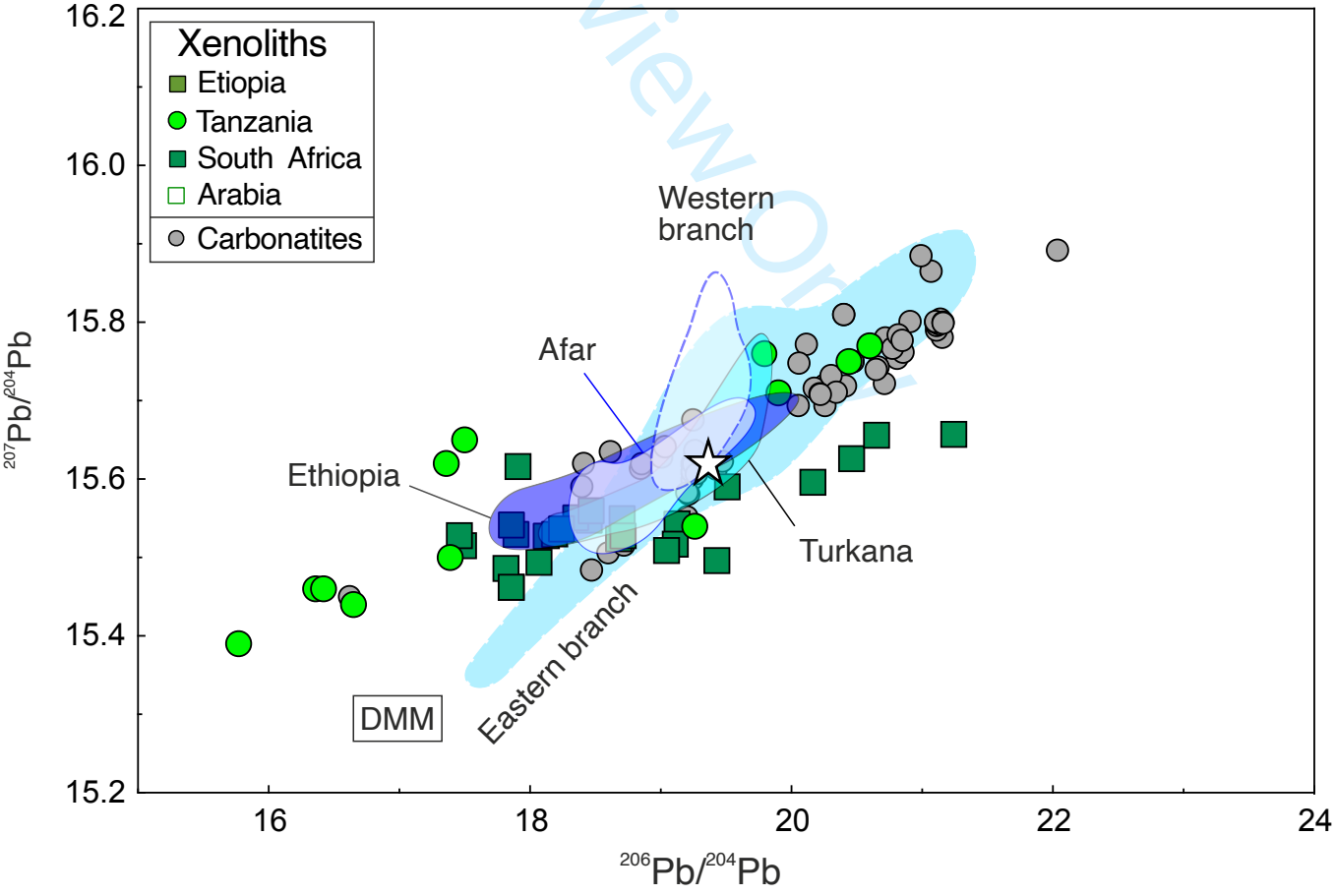

Figure 11

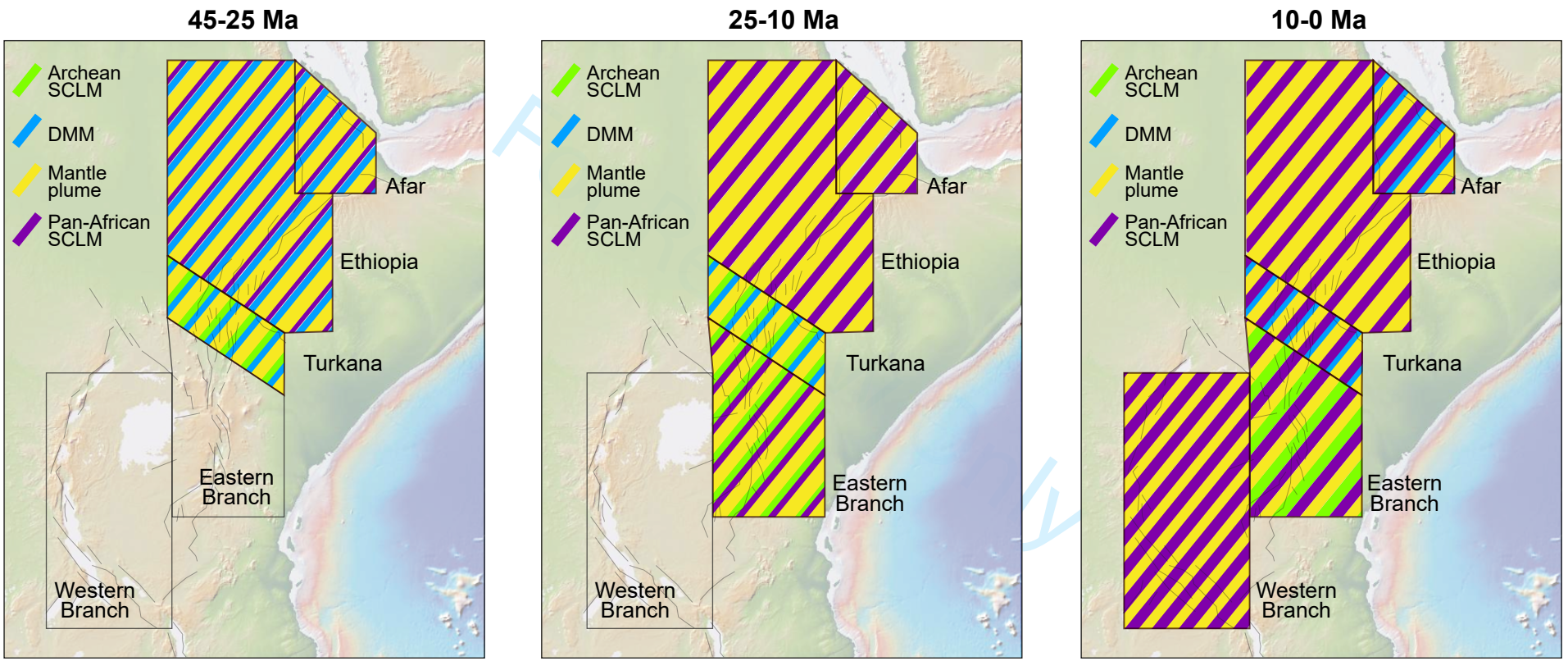
45-25 Ma
25-10 Ma
10-0 Ma
Archean SCLM
DMM
Mantle plume
Pan-African SCLM
Afar
Ethiopia
Turkana
Eastern Branch
Western Branch

Figure 12

Supplementary Material

Analytical methods

A new set of 27 samples were collected from a relatively wide area of the EARS from the Ethiopia (25 samples) and Turkana (2 samples) tectonic domains (Supplementary Table1).

The samples were prepared and powdered for whole-rock characterization of major, trace elements and radiogenic isotopes of Sr and Nd. The reported data are unpublished and presented here for the first time.

Major elements were determined at the Department of Earth Sciences of the University of Florence by X-Ray Fluorescence (XRF), according to the procedure of Franzini et al. (1972). MgO and Na2O were analysed through atomic absorption spectroscopy (AAS) and FeO by tritation. Loss On Ignition (LOI) was determined through gravimetry after heating the sample powders at 950° C.

Trace elements were determined by Inductively Coupled Plasma Mass Spectrometry (ICP-MS) at the Geowissenschaftliches Zentrum der Universitat Gottingen (GZG) on a VG PQ2 system. Analytical uncertainties are within the significant digits reported in Supplementary Table 1.

For isotope analyses, powder digestion and Sr-Nd purification were carried out in the clean laboratory ("Class 1000") of the Department of Earth Sciences of the University of Florence. Sample digestion procedure was performed by sequential HF-HNO3-HCl and elemental separation through specific chromatographic columns, as described in Avanzinelli et al. (2005). All measurements were performed at the Department of Earth Sciences of the University of Florence using a Thermo-Finnigan Triton-Ti® Thermal Ionisation Mass Spectrometer (TIMS), equipped with 9 movable collectors. $^{87}Sr/^{86}Sr$ and $^{143}Nd/^{144}Nd$ were measured dynamically and corrected using an exponential mass fractionation law to $^{86}Sr/^{88}Sr = 0.1194$ and $^{146}Nd/^{144}Nd = 0.7219$, respectively, as described by Avanzinelli et al. (2005). Replicate measurements of NBS 987 and La Jolla reference materials (0.710249 and 0.511856, respectively, Thirlwall 1991) gave mean values of $^{87}Sr/^{86}Sr = 0.710248 \pm 0.000013$ (2s, n = 86) and $^{143}Nd/^{144}Nd = 0.511846 \pm 0.000007$ (2s; n = 67). The Sr procedural blank was 270 pg, which is safely within the blank range of our lab for whole rocks procedures (Avanzinelli et al. 2005).

All data were age corrected to the initial isotope value and errors were fully propagated.

Bibliography

Avanzinelli R., Boari E., Conticelli S., Francalanci L., Guarnieri L., Perini G., Petrone C.M., Tommasini S., Ulivi M. (2005) - High precision Sr, Nd and Pb isotopic analyses using the new generations

Thermal Ionization Mass Spectrometer ThermoFinnigan Triton-Ti, Periodico di Mineralogia 75, 147–166.

Franzini, M., Leoni, L., Saitta, M., 1972. A simple method to evaluate the matrix effect in X-ray fluorescence analyses. X-ray Spectrom. 1, 151–154.

Thirlwall M.F. (1991) - Long-term reproducibility of multicollector Sr and Nd isotope ratio analysis, Chem. Geol. 194, 85–104.

Table S1: Major elements (wt%), trace elements (ppm) and Sr-Nd isotope composition of selected samples.

Sample	*Note*	*Tectonic domain*	*Locality*	*Latitude*	*Longitude*	*Temporal Period*	*SiO_2*	*TiO_2*	*Al_2O_3*	*Fe_2O_3*	*FeO*	*MnO*	*MgO*	*CaO*	*Na_2O*	*K_2O*	*P_2O_5*	*LOI*
Ets 209	1	Ethiopia	Gonder	11°24'58"	37°08'07"	3	44.51	1.78	15.61	4.18	6.40	0.20	11.34	10.08	3.33	1.29	0.30	0.97
Ets 213	1	Ethiopia	Gonder	11°01'30"	36°54'38"	3	46.93	1.32	16.88	2.95	7.20	0.22	7.73	9.38	4.65	1.70	0.35	0.67
Ets 124	3	Ethiopia	Gibat	8°45'00"	37°26'55"	3	42.21	2.72	14.67	2.16	9.10	0.18	11.87	10.72	3.08	0.97	0.83	1.49
Ets 126	3	Ethiopia	Wenchi	8°51'45"	37°43'30"	3	47.48	1.69	16.75	6.49	3.32	0.16	9.12	9.80	2.32	0.97	0.48	1.41
Ets 145	3	Ethiopia	Wechacha	9°04'00"	38°44'00"	3	46.27	1.73	15.60	2.25	7.90	0.16	10.94	9.45	2.88	0.74	0.45	1.62
Ets 161	3	Ethiopia	Wenchi	8°58'25"	37°45'40"	3	46.76	2.02	17.09	2.63	6.52	0.16	8.19	10.84	3.08	1.25	0.59	0.87
Ets 162	3	Ethiopia	Gibat	8°45'25"	37°27'00"	3	45.63	2.19	17.34	1.78	8.20	0.17	9.55	10.06	2.70	0.87	0.46	1.06
Ets 183	3	Ethiopia	Wechacha	9°03'50"	38°28'15"	3	48.59	1.77	17.90	1.66	7.34	0.16	6.80	7.78	4.41	1.56	0.92	1.11
Ets 21	3	Ethiopia	Debre Zeyt	8°50'45"	38°55'45"	3	49.53	2.34	17.73	2.54	8.10	0.17	4.81	8.64	3.35	1.06	0.74	1.00
Ets 243L	1	Ethiopia	Wollega	9°01'31"	36°09'59"	3	43.79	2.96	14.87	3.74	7.20	0.19	10.25	10.54	3.90	1.60	0.62	0.35
Ets 25	3	Ethiopia	Wechacha	8°53'25"	38°39'05"	3	50.00	2.60	18.41	2.57	7.36	0.16	4.36	7.65	3.95	1.27	0.68	1.00
Ets 39	3	Ethiopia	Wenchi	8°53'50"	37°59'20"	3	49.01	2.20	17.52	7.43	3.36	0.19	4.78	9.08	3.74	1.31	0.75	0.63
Ets 43	3	Ethiopia	Gibat	8°44'45"	37°28'05"	3	46.32	2.86	17.10	1.93	8.12	0.18	7.33	9.99	3.23	1.23	0.65	1.06
Ets 48	3	Ethiopia	Nekemt	8°49'25"	36°36'30"	3	44.93	3.08	15.49	2.30	8.96	0.17	7.69	10.61	2.28	1.38	0.63	2.47
Ets 62	3	Ethiopia	Debre Zeyt	8°39'00"	39°10'05"	3	48.62	1.75	16.81	3.84	6.46	0.19	7.13	9.74	2.89	0.84	0.60	1.14
Ets 81	3	Ethiopia	TulluWellel	8°56'30"	35°13'20"	3	49.09	2.61	16.10	3.38	9.20	0.20	5.41	8.18	3.24	0.73	0.47	1.38
Ets 84	3	Ethiopia	TulluWellel	8°56'30"	34°48'10"	3	51.58	2.73	16.20	4.93	5.00	0.22	4.38	6.55	4.49	1.84	1.48	0.60
Ets 241	3	Ethiopia	Arjo-Nekemt	08°51'53''	36°28'39''	2	50.82	2.56	16.31	1.32	10.24	0.19	4.71	7.66	3.57	1.11	0.51	1.01
Ets 281	3	Ethiopia	Guraghe	08°27'05''	38°15'19''	2	47.68	2.94	15.42	5.85	8.64	0.21	4.69	7.86	3.43	0.79	0.98	1.49
Ets 267	3	Ethiopia	Injbara (Tana)	11°24'58''	37°08'07''	2	48.76	1.33	17.95	0.09	8.80	0.15	9.52	8.73	3.10	0.86	0.24	0.48
AA3	2	Ethiopia	Debre Zeyt	8°43'25"	38°59'0"	2	47.03	1.90	17.03	3.86	6.20	0.17	8.89	9.93	2.92	1.18	0.51	0.38
Ets 110	3	Ethiopia	Konchi	8°53'35"	37°00'05"	2	47.13	3.03	16.74	3.97	7.78	0.19	5.27	7.86	4.25	1.63	0.66	1.50
Ets 245	3	Ethiopia	Arjo-Nekemt	08°45'52''	36°29'44''	2	47.02	2.99	17.93	2.18	8.08	0.21	4.39	8.49	4.85	1.79	0.89	1.17
Ets 93	3	Ethiopia	Nekemt	9°06'45"	36°38'30"	1	50.46	3.02	15.02	3.06	9.70	0.21	4.44	7.65	3.20	1.49	0.44	1.32
Ets 108	3	Ethiopia	Konchi	8°50'50"	37°03'05"	1	43.17	2.29	14.60	2.83	7.46	0.16	15.12	8.32	2.89	1.00	0.35	1.81
Etn 9	3	Turkana	Sidamo - Megga	4°03'32"	38°28'48"	3	43.41	2.49	14.13	3.33	8.72	0.19	11.84	9.29	3.87	1.58	0.52	0.62
Etn 13	3	Turkana	Sidamo - Megga	4°07'51"	38°34'48"	3	44.58	2.25	14.14	3.19	9.36	0.23	9.35	8.83	4.58	2.01	0.60	0.88

Footnotes : All isotopic data are unpublished. Notes, 1: major and trace elements from Conticelli et al. (1999), 2: major and trace elements from Gasparon et al. (1993), 3: all data unpublished. Temporal period, 1: 45-

References

Conticelli, S., Sintoni, M. F., Abebe, T., Mazzarini, F., & Manetti, P. (1999). Petrology and geochemistry of ultramafic xenoliths and host lavas from the Ethiopian Volcanic Province: An insight into the upper mantle under eastern Africa. A

Gasparon, M., Innocenti, F., Manetti, P., Peccerillo, A., & Tsegaye, A. (1993). Genesis of the Pliocene to Recent bimodal mafic-felsic volcanism in the Debre Zeyt area, central Ethiopia: Volcanological and geochemical constraints. Journal

Sc	V	Cr	Co	Ni	Zn	Rb	Sr	Y	Zr	Nb	Cs	Ba	Hf	Ta	Pb	Th	U	La	Ce	Nd	Sm	Eu	Gd	Tb	Dy	Ho	Er
n.a.	225	518	53	270	77	95	768	28	167	54	0.90	684	3.94	3.25	1.17	6.33	1.47	43	82	35	6.7	2.2	7.04	0.995	5.65	1.13	3.21
n.a.	164	259	19	130	75	105	901	29	211	136	1.17	994	4.58	7.86	4.68	13.6	3.04	77	131	48	7.8	2.5	8.13	1.02	5.52	1.11	3.19
n.a.	297	524	57	278	n.a.	27	858	29	141	23	0.32	487	2.67	1.6	0.541	4.22	1.1	45	97	48	9.4	3.0	9.29	1.25	6.71	1.25	3.36
n.a.	275	481	50	196	n.a.	22	815	25	156	34	0.098	824	3.78	1.71	2.1	2.81	0.677	26	54	27	5.6	2.0	5.86	0.849	4.87	0.961	2.64
n.a.	248	600	53	291	n.a.	21	626	25	184	42	0.27	335	4.14	2.17	3.81	2.58	0.682	26	55	28	5.8	1.9	6.04	0.868	4.82	0.922	2.46
n.a.	275	330	43	111	n.a.	34	740	30	174	41	0.32	568	4.12	2.04	0.882	4.03	0.934	39	69	34	6.8	2.3	7.18	1	5.53	1.09	2.98
n.a.	345	395	51	147	n.a.	23	735	26	127	44	0.25	369	3.19	2.35	0.696	3.19	0.825	32	64	30	6.0	2.0	6.3	0.885	5.04	0.995	2.73
n.a.	166	143	37	83	n.a.	50	1240	31	325	86	0.61	871	6.49	4.9	5.18	7.73	2.04	65	127	54	9.7	3.1	9.59	1.22	6.23	1.14	3.03
n.a.	336	72	41	25	n.a.	20	746	41	201	39	0.176	502	4.57	2.27	3.62	2.45	0.563	37	63	39	8.1	2.8	8.85	1.28	7.13	1.4	3.85
n.a.	254	281	49	167	83	44	1050	30	274	47	0.48	638	6.07	2.9	1.88	6.47	1.78	59	116	51	9.7	3.1	9.7	1.28	6.76	1.26	3.39
n.a.	270	20	39	17	n.a.	23	1170	45	194	51	0.25	698	4.68	3.28	1.36	3.22	0.863	52	80	54	10.5	3.3	11.2	1.59	9.01	1.82	5.14
n.a.	221	126	40	56	n.a.	25	684	32	249	47	0.26	716	6.01	2.95	1.46	3.19	0.813	42	89	47	9.4	3.3	9.46	1.33	7.31	1.41	3.81
28	314	248	44	82	n.a.	30	976	30	193	61	0.28	494	4.5	3.13	1.44	4.27	1.17	45	92	43	8.4	2.7	8.49	1.14	6.11	1.17	3.13
26	287	436	50	146	n.a.	49	747	30	216	29	0.36	354	4.95	1.79	0.547	3.81	1.07	37	84	45	9.7	3.1	9.51	1.33	7.11	1.29	3.37
n.a.	260	428	48	128	n.a.	14.7	565	67	155	24	0.071	501	3.92	1.35	0.469	1.84	0.429	57	51	48	9.3	2.9	11.4	1.57	8.82	1.9	5.06
n.a.	323	57	48	27	n.a.	14.3	603	28	161	22	0.53	511	4.37	1.23	1.41	2.11	0.52	25	57	32	7.2	2.5	7.35	1.08	6.13	1.2	3.24
n.a.	146	8	22	3	n.a.	33	1300	53	408	24	0.26	716	8.82	1.29	2.68	6.99	2.17	76	179	95	19.0	5.7	18.2	2.36	12	2.18	5.69
n.a.	300	52	39	19	n.a.	20	625	32	174	22	0.155	692	4.44	1.15	2.73	2.08	0.502	26	59	33	7.5	2.7	7.75	1.13	6.32	1.23	3.33
n.a.	335	23	49	43	n.a.	15	546	48	324	27	0.206	342	7.59	1.38	1.93	2.01	0.573	28	68	42	10.1	3.2	10.6	1.61	9.33	1.85	5.06
n.a.	204	296	45	163	n.a.	21	449	22	105	19	0.19	284	2.8	0.84	n.a.	1.73	0.454	15	31	17	3.9	1.41	4.45	0.71	4.31	0.887	2.43
n.a.	249	398	n.a.	119	n.a.	31	638	24	172	42	0.37	444	4.47	2.84	0.343	3.05	0.814	32	67	32	6.6	2.2	6.76	0.961	5.34	1.05	2.87
n.a.	259	17	39	12	n.a.	39	1030	31	255	63	0.43	658	6.71	4.05	3.5	5.22	1.27	50	104	50	9.9	3.1	9.87	1.34	7.06	1.33	3.59
n.a.	188	22	31	20	n.a.	52	1470	37	316	36	0.53	657	6.89	1.82	2.45	7.72	2.31	67	139	64	12.2	3.9	12	1.58	8.24	1.53	4.14
n.a.	350	22	45	13	n.a.	38	619	40	324	51	0.46	567	7.91	2.96	5.83	5.04	1.28	44	97	48	10.0	3.0	10	1.44	7.89	1.54	4.18
n.a.	337	110	48	39	n.a.	32	801	27	169	51	0.293	547	4.46	2.96	1.52	4.28	0.987	38	78	37	7.5	2.4	7.65	1.07	5.93	1.14	3.08
n.a.	232	476	57	349	92	49	875	26	170	41	0.52	621	3.71	2.69	1.17	5.59	1.33	48	96	44	8.5	2.8	8.58	1.15	6	1.1	2.86
n.a.	178	473	45	245	103	70	1080	34	317	90	0.79	761	6.84	5.58	2.77	7.83	1.97	60	117	51	9.7	3.2	9.85	1.31	6.93	1.29	3.43

25 Ma, 2: 25-10 Ma, 3: <10Ma. n.a. = not analyzed, m=measured, i=initial. 2 s.e. = 2* standard error of the mean

\cta Vulcanologica, 11, 143-160.
of African Earth Sciences (and the Middle East), 17(2), 145-165.

Tm	Yb	Lu	$(^{87}Sr/^{86}Sr)_m$	2 s.e.	$(^{87}Sr/^{86}Sr)_i$	2 s.e.	$(^{143}Nd/^{144}Nd)_m$	2 s.e.	$(^{143}Nd/^{144}Nd)_i$	2 s.e.
0.444	2.8	0.431	0.703165	± 0.000007	0.703159	± 0.000007	0.512923	± 0.000005	0.512922	± 0.000005
0.448	2.96	0.468	0.703094	± 0.000006	0.703061	± 0.000006	0.512886	± 0.000006	0.512881	± 0.000006
0.426	2.65	0.396	0.703300	± 0.000006	0.703298	± 0.000006	0.512852	± 0.000005	0.512851	± 0.000005
0.359	2.23	0.34	0.704506	± 0.000006	0.704505	± 0.000006	0.512835	± 0.000005	0.512834	± 0.000005
0.328	2.02	0.307	0.703480	± 0.000008	0.703479	± 0.000008	0.512863	± 0.000005	0.512862	± 0.000005
0.39	2.35	0.366	0.703320	± 0.000007	0.703314	± 0.000007	0.512898	± 0.000005	0.512895	± 0.000005
0.364	2.26	0.345	0.703415	± 0.000008	0.703404	± 0.000008	0.512801	± 0.000004	0.512794	± 0.000004
0.389	2.42	0.364	0.703556	± 0.000007	0.703542	± 0.000007	0.512828	± 0.000006	0.512822	± 0.000006
0.506	3.19	0.491	0.704071	± 0.000007	0.704070	± 0.000007	0.512803	± 0.000005	0.512802	± 0.000005
0.44	2.67	0.405	0.703336	± 0.000006	0.703335	± 0.000006	0.512856	± 0.000006	0.512855	± 0.000006
0.727	4.72	0.758	0.703780	± 0.000008	0.703779	± 0.000008	0.512776	± 0.000006	0.512775	± 0.000006
0.502	3.09	0.472	0.703572	± 0.000007	0.703571	± 0.000007	0.512817	± 0.000004	0.512816	± 0.000004
0.404	2.48	0.371	0.703396	± 0.000006	0.703394	± 0.000006	0.512780	± 0.000006	0.512779	± 0.000006
0.429	2.53	0.367	0.703239	± 0.000007	0.703185	± 0.000008	0.512839	± 0.000006	0.512822	± 0.000006
0.61	3.33	0.525	0.704717	± 0.000008	0.704695	± 0.000008	0.512730	± 0.000005	0.512714	± 0.000005
0.439	2.71	0.416	0.703782	± 0.000006	0.703773	± 0.000006	0.512737	± 0.000004	0.512728	± 0.000004
0.704	4.24	0.628	0.703548	± 0.000008	0.703535	± 0.000008	0.512773	± 0.000005	0.512762	± 0.000005
0.441	2.81	0.427	0.703970	± 0.000007	0.703961	± 0.000007	0.512712	± 0.000005	0.512706	± 0.000005
0.689	4.3	0.661	0.703798	± 0.000008	0.703793	± 0.000008	0.512764	± 0.000007	0.512759	± 0.000007
0.342	2.13	0.327	0.703388	± 0.000007	0.703373	± 0.000007	0.512889	± 0.000005	0.512881	± 0.000005
0.389	2.44	0.369	0.703867	± 0.000006	0.703865	± 0.000006	0.512820	± 0.000004	0.512819	± 0.000004
0.465	2.86	0.429	0.703507	± 0.000007	0.703495	± 0.000007	0.512779	± 0.000004	0.512773	± 0.000004
0.531	3.35	0.5	0.703129	± 0.000007	0.703128	± 0.000007	0.512877	± 0.000005	0.512877	± 0.000005
0.554	3.45	0.521	0.703949	± 0.000006	0.703929	± 0.000006	0.512722	± 0.000004	0.512716	± 0.000004
0.402	2.5	0.373	0.703522	± 0.000006	0.703514	± 0.000006	0.512764	± 0.000006	0.512760	± 0.000006
0.361	2.19	0.322	0.703060	± 0.000006	0.703057	± 0.000006	0.512918	± 0.000004	0.512917	± 0.000004
0.447	2.78	0.418	0.703039	± 0.000006	0.703036	± 0.000006	0.512924	± 0.000005	0.512923	± 0.000005